2013

Screening Of Quantum Dots For Toxicity On The Growth And Viability Of Escherichia Coli

Jeremy Tharkur
University of Central Florida

SCREENING OF QUANTUM DOTS FOR TOXICITY ON THE GROWTH AND VIABILITY OF *ESCHERICHIA COLI*

by:

JEREMY THARKUR
B.S, University of South Florida, 2011

A thesis submitted in partial fulfillment of the requirements
for the degree of Master of Science
in the Department of Molecular Biology and Microbiology
in the Burnett school of Biomedical Science
in the College of Medicine
at University of Central Florida
Orlando, Florida

Fall Term
2013

Major Professor: Swadeshmukul Santra

ABSTRACT

Heavy metal (HM) containing quantum dots (Qdots) are increasingly used in commercial products due to their unique electronic, optoelectronic, optical and magnetic properties. Once disposed to the landfill, environmental weathering is likely to compromise HM Qdot integrity, leading to release of heavy metal ions. To minimize any negative environmental impact of HM Qdots, there is an increasing demand for developing HM free or environmentally-friendly surface modified HM Qdot alternatives. In this study, synthesis of HM free ZnS:Mn/ZnS and surface modified HM CdS:Mn/ZnS Qdots (using N-acetylcysteine, NAC, and Dihydrolipoic acid, DHLA) and their potential toxicity assessment using *E. coli* as a model system is reported. NAC and DHLA are known antioxidants and therefore expected to reduce HM induced toxicity and improve colloidal stability of Qdots. All Qdots were synthesized at room temperature using a reverse micelle microemulsion method. Qdots were fully characterized using UV-visible absorption spectroscopy, fluorescence emission spectroscopy, zeta potential, Nuclear Magnetic Resonance spectroscopy (NMR) and High Resolution Transmission Electron Microscopy (HRTEM). Qdot environmental weathering was simulated by treating Qdots with concentrated acid (6N HCl). Qdot toxicity was evaluated on *E. coli* growth and viability using growth curves, turbidity and bactericidal assays (CFU). Results show that Zn based Qdots exhibit reduced toxicity on *E.coli* growth and viability when compared to Cd based Qdots. In addition, surface modification with NAC and DHLA minimized toxicity of Cd based Qdots. In summary, Zn based Qdots appear to be more environmental-friendly than Cd based Qdots.

I dedicate this work to Glen and Eileen, Adam, Daniel, Serena and Melanie

ACKNOWLEDGMENTS

I am grateful for my professor, Swadeshmukul Santra, PhD, for his guidance and commitment to my research. I also acknowledge my committee professors, William Self, PhD and Sean Moore, PhD, for their support and valuable suggestions towards improving my work.

I owe a lot of my accomplishments to my colleagues and lab mates, Karishma Cantarero, Andrew Teblum, Jen Archer, Srijita Basumalick, Megan Berroth, Josh Bazata, and especially Parthiban Rajasekaran and Mikaeel Young. Their knowledge, expertise, support and presence will never be forgotten. I thank my friends Almatmed Abdelsalam, Nickisha Pierre-Pierre, Mona Matthew and Nathan Roney.

Thank you to Ernie Gemeinhart, Diane Maldonado, Ushaben Lal, Mari Pina, and the rest of the NSTC staff for their availability and assistance. I appreciate the contributions from Helge Heinrich, PhD, Kirk Scammon, and the UCF-Materials Characterization Facility (MCF) for helping with materials characterization. I greatly appreciate David Richardson, PhD for taking the time to train me in NMR, and Dr. Qun Huo, PhD for assisting me with Zeta potential.

Most importantly I thank my family for their love and faith in me. A special thanks to Melanie Suaris, my wonderful parents, Glen and Eileen Tharkur, and my dependable brother, Adam Tharkur.

The research was funded by National Science Foundation, grant number 1159500.

TABLE OF CONTENTS

LIST OF FIGURES viii

LIST OF TABLES xii

LIST OF EQUATIONS xiii

CHAPTER 1- BACKGROUND AND SIGNIFICANCE 1

CHAPTER 2- MATERIALS AND METHODS 6

2.1 Materials 6

2.2 Instrumentation 6

2.3 Methods 7

2.3.1 CdS:Mn/ZnS and ZnS:Mn/ZnS Quantum Dots 7

2.3.2 Purification 8

2.3.3 Coating 9

2.3.4 Nanoparticle Characterization 10

2.4 Bacterial Assays 13

2.4.1 Growth Curves and Endpoint Turbidity 14

2.4.2 Bactericidal Assays 14

CHAPTER 3- RESULTS AND DISCUSSION 15

3.1 Absorbance and Photoluminescence Characterization 15

3.2 Zeta Potential 16

3.3 Surface Functionality Characterization 17

3.4 High Resolution Transmission Electron Microscopy.....18

3.5 Compromised Quantum Dots.....19

3.6 Bacterial Toxicity.....19

CHAPTER 4- CONCLUSION.....59

REFERENCES.....60

LIST OF FIGURES

Figure 1- Fluorescence Emission of CdS:Mn/ZnS Qdots by handheld UV light source.....22

Figure 2- Fluorescence Emission of ZnS:Mn/ZnS Qdots by handheld UV light source.....22

Figure 3- UV-Visible spectroscopy of coated and uncoated CdS:Mn/ZnS Qdots in DI water.....23

Figure 4- UV-Visible spectroscopy of coated and uncoated ZnS:Mn/ZnS Qdots in DI water.....23

Figure 5- Normalized fluorescence spectroscopy of coated and uncoated CdS:Mn/ZnS Qdots in DI water. Excitation λ: 375nm.....24

Figure 6 – Normalized fluorescence spectroscopy of coated and uncoated ZnS:Mn/ZnS Qdots in DI water. Excitation λ: 308nm.....24

Figure 7- Nuclear Magnetic Resonance Spectroscopy of AOT 27

Figure 8- Nuclear Magnetic Resonance Spectroscopy of N-acetylcysteine 27

Figure 9- Nuclear Magnetic Resonance Spectroscopy of Lipoic Acid.....27

Figure 10- Nuclear Magnetic Resonance Spectroscopy of bare CdS:Mn/ZnS Qdots 28

Figure 11- Nuclear Magnetic Resonance Spectroscopy of NAC coated CdS:Mn/ZnS Qdots.....28

Figure 13- Nuclear Magnetic Resonance Spectroscopy of bare ZnS:Mn/ZnS Qdots 29

Figure 14- Nuclear Magnetic Resonance Spectroscopy of NAC coated ZnS:Mn/ZnS Qdots.....29

Figure 15- Nuclear Magnetic Resonance Spectroscopy of DHLA coated ZnS:Mn/ZnS Qdots ...29

Figure 16- Energy-dispersive X-ray spectroscopy (EDX) for elemental analysis of 30

Figure 17-HR-TEM (low mag) image of NAC coated CdS:Mn/ZnS Qdots with scattered dark contrast confirming the presence of electron-rich material 31

Figure 18- HR-TEM (high mag) image of NAC coated CdS:Mn/ZnS Qdots with scattered dark contrast confirming presence of electron-rich material 32

Figure 19- Selected area electron diffraction (SAED) image during HR-TEM of.....33

Figure 20- Energy-dispersive X-ray spectroscopy (EDX) for elemental analysis of DHLA coated CdS:Mn/ZnS Qdots during HR-TEM 34

Figure 21-HR-TEM (low mag) image of DHLA coated CdS:Mn/ZnS Qdots with scattered dark contrast confirming presence of electron-rich material 35

Figure 22- HR-TEM (high mag) image of DHLA coated CdS:Mn/ZnS Qdots with scattered dark contrast confirming presence of electron-rich material 36

Figure 23- Selected area electron diffraction (SAED) image during HR-TEM of.....37

Figure 24- Energy-dispersive X-ray spectroscopy (EDX) for elemental analysis of NAC coated ZnS:Mn/ZnS Qdots during HR-TEM 38

Figure 25-HR-TEM (low mag) image of NAC coated ZnS:Mn/ZnS Qdots with scattered dark contrast confirming presence of electron-rich material 39

Figure 26- HR-TEM (high mag) image of NAC coated ZnS:Mn/ZnS Qdots with scattered dark contrast confirming presence of electron-rich material 40

Figure 27- Selected area electron diffraction (SAED) image during HR-TEM of.....41

Figure 29-HR-TEM (low mag) image of DHLA coated ZnS:Mn/ZnS Qdots with scattered dark contrast confirming presence of electron-rich material 43

Figure 30- HR-TEM (high mag) image of DHLA coated ZnS:Mn/ZnS Qdots with scattered dark contrast confirming presence of electron-rich material 44

Figure 31- Selected area electron diffraction (SAED) image during HR-TEM of.....45

Figure 32- Fluorescence spectroscopy of normal and HCl treated (compromised) CdS:Mn/ZnS Qdots and commercial Qdot 46

Figure 33- Fluorescence spectroscopy of normal and HCl treated (compromised) ZnS:Mn/ZnS Qdots 46

Figure 34- E. coli growth curve comparison between commercial Qdot (CdSe/ZnS) treated and non treated control. 47

Figure 35- *E. coli g*rowth curve comparison with CdS:Mn/ZnS Qdots treated and untreated control.....48

Figure 36- *E. coli* growth curve comparison with ZnS:Mn/ZnS Qdots treated and untreated control.....49

Figure 37- Endpoint turbidity comparison of normal and compromised commercial Qdots 49

Figure 38- Endpoint turbidity comparison of AOT to untreated *E. coli*.....50

Figure 39- Endpoint turbidity comparison of NAC to untreated *E. coli*.....50

Figure 40- Endpoint turbidity comparison of AOT to untreated *E. coli*.....51

Figure 41- Endpoint turbidity comparison of Zinc acetate and Cadmium acetate salts to untreated E.coli 52

Figure 42- Endpoint turbidity comparison of CdS:Mn/ZnS Qdots 53

Figure 43- Endpoint turbidity comparison of compromised CdS:Mn/ZnS Qdots 53

Figure 44- Endpoint turbidity of *E. coli* treated with commercial and synthesized Cadmium based Qdots, both normal and compromised.....54

Figure 45- Endpoint turbidity comparison of ZnS:Mn/ZnS Qdots.....54

Figure 46- Endpoint turbidity comparison of compromised ZnS:Mn/ZnS Qdots.....55

Figure 47- Colony counts of *E. coli* in the presence of normal and compromised commercial Qdots (0.1 μg of metallic cadmium) 55

Figure 48- Colony count of *E. coli* untreated (control) compared to Qdot surface agents and core salts.....56

Figure 49- Colony counts of *E. coli* treated with normal and compromised CdS:Mn/ZnS Qdots56

Figure 50- Colony counts of *E. coli* treated with commercial and synthesized Cadmium based Qdots, both normal and compromised. 57

Figure 51- Colony forming units of *E. coli* treated with ZnS:Mn/ZnS Qdots and compromised ZnS:Mn/ZnS Qdots. 58

LIST OF TABLES

Table 1- Quantum Yield calculations for coated and uncoated CdS:Mn/ZnS Qdots. 24

Table 2- Quantum Yield calculations for coated and uncoated ZnS:Mn/ZnS Qdots. 25

Table 3- Zeta Potential measurements of coated and uncoated CdS:Mn/ZnS 26

Table 4- Zeta Potential measurements of coated and uncoated ZnS:Mn/ZnS 26

LIST OF EQUATIONS

Equation.....**Error! Bookmark not defined.**

CHAPTER 1- BACKGROUND AND SIGNIFICANCE

Quantum dots (Qdots) have been well studied for use in biomedical sciences as biomarkers for cells organelles[1], labeling agents to distinguish between cells [2, 3], delivery vehicles for probing drug delivery and intracellular events [4-7]. Qdots are man-made light emitting semiconductor nanomaterials ranging from 2-10 nanometers in size. Their unique optical and electrical properties (broad absorption with narrow emission, large extinction coefficients, high quantum yield (QY) and resistance to photobleaching [1, 8-11]) make them ideal materials for a wide range of applications. Since Qdots have a broad absorbance with narrow emission, they can be manipulated to fluoresce in different colors using a single excitation source [9]. The fluorescence emission is a result of the energy difference between the valence and conduction bands of the central core. When the electrons are excited from valence band to the conduction, it leaves a hole behind. As the electron returns to its resting state, it emits light energy. The size of the band gap will vary inversely with the physical diameter of the Qdot, therefore that smaller sized Qdots will have a stronger fluorescence [12].

Qdots have core structures composed of metals from the group 2-4 of the transitional metals of the periodic table, with cadmium being the most common. To obtain highly efficient Qdots, the core is passivated by a wide band gap inorganic semiconductor layer (shell). The additional layer eliminates surface defects and confines the charge carriers to the core reducing energy loss [13]. Zinc sulfide is a commonly used semiconductor shell because it possesses a large band gap and is resistant to high electric fields [14, 15]. A second strategy to improve Qdot photoluminescence efficiency is through doping. Doping the central core creates impurities in the crystal structure. These impurities enhance the quantum dot's fluorescence by creating more intermediate band gaps which the electrons can travel through as they return to their resting state.

Mn^{2+} ions are the most commonly used dopants as they possess similar chemical properties to Cd and Zn [16]. The transfer of the electron-hole pair into the Mn^{2+} environment leads to a characteristic yellow-orange emission from the Mn^{2+} $^4T_1$-$^6A_1$ transition [16]. The Qdots used in this research contain cadmium sulfide (CdS) or zinc sulfide (ZnS) semiconductor cores that are doped with Mn^{2+} ions and surface passivated with a ZnS shell (CdS:Mn/ZnS and ZnS:Mn/ZnS, respectively).

The Qdots are synthesized at room temperature in reverse micelle (w/o) microemulsions (ME) following a slightly modified procedure [17]. The ME contains a heptane oil layer and dioctyl sulfosuccinate sodium salt (AOT) surfactant that surrounds the nano-sized water droplets that comprise the water layer. AOT is commonly used surfactant with agricultural, industrial, and biomedical applications. Each water droplet serves as a reaction center for Qdot assembly and growth. The water:oil:surfactant ratio is paramount to controlling the particle size of the Qdots [18, 19]. Instability of the ME leads to surface defects and multiple particle sizes, which could negatively impact the photoluminescence efficiency.

Synthesized Qdots are hydrophobic since they are devoid of hydrophilic surface functional groups. For that reason, Qdots are further modified with an organic layer to promote water dispersability and functionality. Surfactant replacement with a hydrophilic substitute is the most widely used procedure. For example, a surfactant mixture of trioctylphosphine and trioctylphosphine oxide (TOP/TOPO) is slowly exchanged with mercaptopropionic acid (MPA) for transition Qdots of from hydrophobic to hydrophilic. While this established procedure is popularly used to make commercially available Qdots, the significant drawback is the drop in fluorescence intensity [1, 9, 20, 21]. In addition, complete surfactant replacement is never achievable as that would lead to instability of the Qdot.

The functionality of Qdots is results from ligand conjugation to the outermost layer Depending on the ligand, Qdots can be directed to specific organelles or cells in the body; thus utilizing their fluorescence properties for bioimaging and biosensing purposes [1]. The Qdots used in this research have a ZnS outer shell and are bound to ligands via disulfide bonds. This research employs N-acetylcysteine (NAC) and dihydrolipoic acid (DHLA) as the surface modifying ligands. Both NAC and DHLA are known antioxidants [22, 23]. NAC is a precursor to glutathione, an intracellular antioxidant [24]. It is a widely used surface ligand for improving Qdot dispersion in water [25, 26], has shown to inhibit biofilm formation [27, 28], increase bacterial susceptibility to antibiotics [24] and has been employed as a mucolytic reagent for treating chronic obstructive pulmonary disorder (COPD) [22]. Since DHLA is the reduced form of LA [29], both are capable of scavenging hydroxyl radicals, hypoclorous acid, singlet oxygen, peroxynitrite-induced damage [30], and 4-Aminophenol toxicity [31], but only DHLA has exhibited peroxyl radical and superoxide radical scavenging capabilities. Though the antioxidant capabilities of both molecules have been widely studied, some findings have indicated that DHLA and LA may also have some prooxidant properties as well [23].

As the research into Qdot understanding and manipulation improves, many commercial applications develop as well. There are at least 17 companies around the world that manufacture heavy metal (HM) based Qdots commercially. Qdots are currently incorporated as organic light emitting diodes (OLEDs) into lighting displays providing better color purity, longer lifetime, and are more energy and cost efficient than current LEDs on the market. They are used in solar cells to reduce the manufacturing cost while increasing the energy efficiency, and as hydrophobic and hydrophillic printable inks. Other applications range from lasers to anti counterfeiting [32]. Although the main use of HM based Qdots is in biomedical applications the world value of

Qdots is likely to increase to $13 billion in 2014 (Lux Research) indicating that Qdot consumption is rising. Commercialized Qdot OLEDs are already being sold into flat screen displays for televisions. As more commercial applications develop, the value of Qdots will increase to over $2.6 trillion over the next ten years (Lux Research). The United States accounted for $14.9 billion in laptops, $29 billion in tablets and $33.7 billion in smartphones sales in 2012 [33]. At the rate at which Americans consume technological goods, the negative impact of HM toxicity to the environment is likely to increase.

Since Cd based HM Qdots are the most widely commercially distributed Qdots, the impact of Cd based Qdot HM toxicity on bacteria and animals has been widely studied. The drawback to using cadmium-based quantum dots is when Cd^{2+} ions leak into the intracellular environment and disrupt cellular processes at the molecular level. Cd^{2+} ions are known to be toxic and have been classified as a category 1 carcinogen because of the involvement in cancer development [34]. Cd has been found to directly affect DNA by covalently binding to DNA strands, and indirectly through reactive oxygen species production (ROS) and causing DNA-protein and DNA-amino acid crosslinking that inhibits DNA repair mechanisms [34, 35].

Qdot weathering involves the degradation of surface coatings and shell layer passivation. Once released into the environment Qdots are at risk of weathering via environmental conditions that cause pH changes, redox transformations, and photolysis [36]. The main toxic effect has been attributed to the release of Cd^{2+} ions from weathered Qdots which produce ROS [37], and according to published literature, Cd^{2+} ion release occurred for weathered Qdots at $pH< 6$ [38, 39]. The release of Cd^{2+} ions will have a direct negative effect on the surrounding ecosystem encompassing both bacteria [37-40] and eukaryotic organisms [36]. Because of the sensitive nature of Qdots, finding ways to reduce HM ion availability to biological systems will

significantly reduce the potential toxicity [41]. As a result, recent research has shifted to developing methods that involve HM free metal cores and developing core shells to prevent ion leakage.

Since Zn is an essential micronutrient for both bacteria and mammalian species [42], the toxic effect should be significantly reduced when compared to Cd based HM Qdots. In this research, HM free Zn based Qdots were investigated for their potential for replacing HM Qdots. In addition, the research studied the efficiency of antioxidant molecules on reducing HM toxicity. Toxicity was assessed using *E. coli* as the model organism. Toxicity to viability and growth of *E. coli* was evaluated using growth curves, turbidity assays, and bactericidal assays. Taken together, this research presents potential replacements to HM Qdots that exhibit decreased biological toxicity after weathering.

CHAPTER 2- MATERIALS AND METHODS

2.1 Materials

All reagents were purchased at reaction grade purity from commercial vendors and used without any additional purification unless stated specifically. Cadmium Acetate Dihydrate (Acros), Zinc Acetate dehydrate (Sigma), Manganese Acetate Tetrahydrate (Acros), Sodium Sulfide (Sigma), Dioctyl Sulfosuccinate Sodium Salt (AOT, Acros), HPLC Grade Heptane (Fisher), N-Acetyl-L-Cysteine (NAC, Acros), (±)- a - Lipoic acid (LA, Sigma), Ethanol 95% (Fisher), Sulfuric Acid (provided by the Chemistry Department, University Central Florida), Acetone (VWR), Deuterium Oxide for NMR 99.8% (Acros), Methyl Sulfoxide-d6, NMR (Acros), Sodium Borohydride (Sigma), Phosphate Buffer Saline 10X (PBS, Cellgro), Luria-Bertani Broth and Agar (LB, Fluka), Hydrochloric Acid (HCl, Fisher), Quinine Sulfate Dihydrate (Acros). Deionized Water (DI) was obtained from Nanopure(Barnstead Model # D11911)

2.2 Instrumentation

Qdot fluorescence was visualized using a hand-held UV excitation source (Mineralight®, multiband UV 254/365nm lamp, Model UVGL-58). All fluorescence emission and UV-Visible absorbance spectra were collected using a NanoLog Spectrofluorimeter (SPEX, Jobin Yvon

Horiba) and a Cary 300 UV-VIS Spectrophotometer, respectively. Electrophoretic mobility was measured by zeta potential using a Malvern Zetasizer Nano ZS90. Surface functionality was characterized by Nuclear Magnetic Resonance (NMR) using a Varian NMR Systems 500Mz. Qdot crystal size, crystallinity, and elemental analysis characterizations were completed using a FEI Technai F30 TEM. Optical density (OD) readings for turbidity assays and growth curves were measured using a SpectraMax 190 plate reader (Molecular Devices).

2.3 Methods

2.3.1 CdS:Mn/ZnS and ZnS:Mn/ZnS Quantum Dots

2.3.1.1 Synthesis

Quantum dots were synthesized at room temperature using a modified reverse micelle water-in-oil (w/o) microemulsion protocol [13]. Three flasks (A, B, C) were washed with soap, then acid washed with 1% hydrochloric acid (HCl), and dried at 150°C to dissolve any contaminants and remove all water from the glassware. To flasks A, B, and C, 25mL, 75mL, and 75mL of Heptane were added respectively and mixed with 2.23g, 6.69g, and 6.69g of dioctyl sulfosuccinate sodium salt (AOT) respectively for 30min using magnetic stirrers. In vial A, 266mg of cadmium acetate dihydrate and 4.78 mg of manganese acetate tetrahydrate were dissolved in 10mL of deionized water (DI). Vial B contained 257.5mg of sodium sulfide dissolved in 5mL DI water. Vial C contained 285.25mL zinc acetate dihydrate dissolved in 5mL DI water.

Once the AOT was completely dissolved in heptane, 2.7mL of Vial B were added to Flask B and mixed for 1 hour. After the first 30min, 900μL of Vial A were added to Flask A and mixed for the remaining 30min. When 15min had elapsed, 2.7 mL of Vial C were added to Flask C and mixed for 30 min. After Flask A and Flask B had completed their individual mixing times, the contents of Flask A were poured into Flask B and an immediate yellow color change occurred. There was no color change during the ZnS:Mn/ZnS Qdot synthesis. The new solution of A and B was allowed to mix for 15min. After 15min, Flask C was added to the solution containing A and B using a burette at a rate of 1-2mL/min. Fluorescence was visibly detected using long wave excitation from a handheld multiband UV 254/365nm lamp. The final solution was protected from light using aluminum foil and left to stir for at least 48hours before analysis or further modification.

ZnS:Mn/ZnS quantum dots were synthesized using the same procedure mentioned previously with vial A containing 213mg of zinc acetate dihydrate and 3.83mg manganese acetate tetrahydrate. Fluorescence emission was observed using short wave excitation from the handheld multiband UV 254/365nm lamp.

2.3.2 Purification

Bare quantum dots in microemulsion (10ml) were removed from the stock solution and added to a 50mL conical centrifuge tube. In order to break apart the microemulsion, 20mL of a 1:1 acetone/95% ethanol solution were added to the 50mL conical centrifuge tube and then centrifuged at 11,000 rpm for 5 minutes. The fluorescent pellet was visualized using the

handheld multiband UV 254/365nm lamp and the nonfluorescent supernatant was discarded. The pellet was washed three times in 10mL of acetone, twice in 10mL heptane, and then once more in 10mL acetone. In between each wash the pellet was sonicated for 5 mins. Each wash was done at 11,000 rpm for 5min. After the final acetone wash, the nonfluorescent supernatant was discarded and the residual acetone was evaporated using a hot water bath for 5-10min. The dry pellet weight was measured and then re-dispersed in DI water. The fluorescent solution was shaken to check for residual AOT. Water washes were repeated as necessary to remove additional AOT.

2.3.3 Coating

2.3.3.1 N-Acetyl-L-Cysteine

AOT (0.892g) was dissolved in heptane (10mL) for 30min using a magnetic stirrer. During that time, 50mg of NAC was dissolved in 1mL of DI water. When the time elapsed, 360μL of the dissolved NAC was added dropwise into the stirring heptane solution. After 30min, 10mL of Qdots in microemulsion were added to the stirring NAC microemulsion dropwise. The final combined microemulsion was left to magnetically stir overnight and then purified by the previously mentioned procedure. The newly coated Qdots were then stored at 4°C.

2.3.3.2 Dihydrolipoic Acid

Washed bare Qdots in DI water (20mLs) were cooled to 4°C while magnetically stirring in a glass vial. 50mg of Lipoic Acid (LA) were added to the cold Qdots and the solution was sonicated for 5min. After sonication, the vial was cooled back to 4°C. After confirming the temperature with a thermometer, 200mg of sodium borohydride was added and the vial was covered and left to magnetically stir for 1 hour. DHLA coated Qdots were dialyzed for 48 hours in DI Water. The DI water was replaced every 6 hours to facilitate removing the sodium borohydride. The newly coated, purified Qdots were stored at 4°C.

2.3.4 Nanoparticle Characterization

2.3.4.1 UV-Visible Spectroscopy

UV-Visible spectroscopy samples were analyzed using 3mL quartz cuvettes. The instrument was blanked against DI water before each sample. Sample absorbance were measured from 800-200nm and diluted appropriately until peak absorbance was 0.1 at 375nm and 308nm for CdS:Mn/ZnS and ZnS:Mn/ZnS Qdots, respectively. All samples were measured using DI water.

2.3.4.2 Fluorescence Spectroscopy

The NanoLog Spectrafluorometer was first calibrated with DI water in a completely transparent quartz cuvette to measure the water ramen emission. The water raman spectra exhibited a proper Gaussian curve with peak maxima appearing at 397nm and intensity above 200,000 arbitrary units (A.U.). After standardizing the UV-Visible absorbance for each Qdot, each sample's fluorescence emission was measured in DI water with 375nm and 308nm excitation for CdS:Mn/ZnS and ZnS:Mn/ZnS Qdots, respectively.

2.3.4.3 Quantum Yield

Quantum Yield (QY) values were calculated using single-point quantum yield comparison. (Equation 1[43]) for bare and coated Qdots in water. Φ_x and Φ_R represent the QY of the sample and reference respectively. I represents the integrated fluorescence emission. OD represents the optical density (OD). UV-Visible spectroscopy data was measured for quinine sulfate in 0.05M sulfuric acid and CdS:Mn/ZnS and ZnS:Mn/ZnS Qdots in water. Quinine sulfate was standardized to an absorbance intensity of 0.1 at 375 to compare with the CdS:Mn/ZnS Qdots, and 308nm to compare with ZnS:Mn/ZnS Qdots. After measuring the absorbance, the fluorescence emission of each sample was measured and the spectra were integrated for the QY calculation. The index of refraction for water and sulfuric acid are 1.33 and 1.37 respectively.

2.3.4.4 Zeta Potential

Samples were prepared by transferring 700ul of Qdot samples in DI water (1mg/mL) into disposable Zetasizer capillary cuvettes. Zeta potential for each sample was measured in triplicate. Temperature was held constant at 25°C. The dielectric constant of the medium was 78.6.

2.3.4.5 Nuclear Magnetic Resonance Spectroscopy

Washed Qdot samples were frozen overnight and then lyophilized to a dry powder. The dry weight was measured and then each sample was re-dispersed in the appropriate deuterated solvent. NAC was dispersed in deuterium oxide. Lipoic acid and AOT controls were dispersed in and methyl sulfoxide-d6. Proton NMR spectra were collected and analyzed. Pulse sequence parameters included a relax delay of 1 second, 45° pulse, 4.089 sec acquisition time, and 32 repetitions. Temperature was maintained at 25°C.

2.3.4.6 High Resolution Transmission Electron Microscopy

Carbon coated copper grids- 400 mesh (Electron Microscopy Sciences) were submerged in surface modified quantum dots of both Cds:Mn/ZnS and ZnS:Mn/ZnS Qdots in DI water for 20-30min and then placed on a Kimwipe in a plastic petri dish to dry overnight. Grids were carried to UCF-AMPAC-MCF for HRTEM analysis. Measuring crystal size and lattice spacing, visualizing the crystallinity, and elemental analysis were all completed at UCF-AMPAC-MCF.

2.3.4.7 Compromised Qdots

To compromise the Qdot integrity, 30µL of 6N HCl was added to 1mL of Qdots. Fluorescence quenching was monitored using the Nanolog Fluorescence Spectrophotometer. Complete quenching of fluorescence emission confirmed that the integrity of the Mn^{2+} dopant core had been compromised. For bacterial toxicity evaluation, the pH of each sample was neutralized by titrating with 6M NaOH. The pH changes were monitored using a pH meter. Final pH of the Qdot samples ranged from 7.05-7.4. DI water was treated similarly and final pH was measured at 7.13.

2.4 Bacterial Assays

Escherichia coli (*E.coli*) ATCC 35218 was received from the Microbiology lab at University of Central Florida. Culture stocks were grown using Luria Bertani (LB) broth. Individual bacteria colony isolation was done on LB agar plates. Before each experiment, a single colony of bacteria was transferred into 10mL of freshly made LB broth and incubated at 37°C overnight. All bacterial manipulations were done inside a sterilized laminar flow. Sterility was maintained by using autoclaved microcentrifuge tubes and micropipette tips. All bacterial assays were run in triplicates for each sample.

2.4.1 Growth Curves and Endpoint Turbidity

E.coli OD was standardized to 0.5 McFarland using a McFarland standard kit (Fisher). 900µL of Qdot samples was added to 100µL of 10X Phosphate Buffer Saline (PBS) to create stocks of Qdots in 1X PBS and stored in sterile 1.5mL microcentrifuge tubes. Samples were measured in triplicate using sterile 96-well plates. Each well was prepared using 100µL serial dilutions of each Qdot in 1X PBS and 100µL of bacteria cells in LB broth. Final well volume was maintained at 200µL. OD_{600} was collected every hour for 24 hr at 37°C inside a SpectraMax 190 plate reader (Molecular Devices). Endpoint turbidity was measured as absorbance at OD_{600} after 24 hrs of bacterial growth.

2.4.2 Bactericidal Assays

Qdot samples (normal and compromised, 1mg/mL) in 1x PBS were incubated with bacteria in LB broth for 24 hrs at 37°C in 96-well plates as mentioned previously. After 24 hrs, 100µL of each sample was added to 900µL of sterile 1x PBS (pH 7.4) using sterile microcentrifuge tubes. Serial dilutions were made from 10^{-1} to 10^{-8}. Freshly prepared LB agar plates were divided into four quadrants and labeled -5, -6, -7, and -8. Five 10µL drops of the 10^{-8} dilution were placed onto the plate in the quadrant labeled -8. This was repeated for each consecutive dilution for their respectively labeled quadrant. The prepared plates were allowed to dry before inverting and then placed in an incubator overnight (15-16 hours). Colony counts were verified for reliability by ensuring that the number of colonies in the lower dilution were one-tenth the number of colonies in the immediate higher dilution.

CHAPTER 3- RESULTS AND DISCUSSION

3.1 Absorbance and Photoluminescence Characterization

CdS:Mn/ZnS and ZnS:Mn/ZnS Qdots (bare and surface modified) were initially visualized using a handheld UV light source to confirm the bright fluorescence of the Qdots (**Figure 1 and 2**). The 365nm excitation (long wave) of the CdS:Mn/ZnS Qdots shows the bright yellow-orange emission of the Qdots that results from the Mn^{2+} $^4T_1$-$^6A_1$ energy band gap. The 254nm excitation (short wave) of the bare ZnS:Mn/ZnS Qdots does not show the same bright yellow-orange emission due to potential surface defects. Further surface modification allows for the bright yellow-orange fluorescence. Particle aggregation for the bare and water dispersion for the surface modified Qdots were also visible.

UV-visible absorption (**Figure 3 and 4**) for the bare quantum dots show the light scattering effect occurring as a result of the aggregated Qdots. As opposed to the bare Qdots, the surface modified Qdots do not exhibit the same light scattering since they are not as aggregated. In addition, surface modification increased the Qdot absorbance in the UV range.

Normalized fluorescence emission of the CdS:Mn/ZnS bare, NAC coated, and DHLA coated and ZnS:Mn/ZnS bare, NAC coated, and DHLA coated Qdots (**Figure 5 and 6)** show slight shifts in peak position (590, 587, 591, 591, 588, and 593 nm, respectively) due to the surface modification, however the Mn dopant environment was not compromised since there are no significant differences between the Qdots. In addition, the full width at half maxima (FWHM) for each respective type of Qdot was almost identical indicating that the emission was not due to any secondary fluorophores in the nanoparticles. Since the excitation wavelength for the

ZnS:Mn/ZnS Qdots was 308nm, the second harmonic of the excitation occurred at 616nm and masked the down sloping red region of the emission spectra. However, the integrity of the Mn dopant environment was maintained as evidenced by the ~590 peak position is each sample, indicating that the Qdots were not affected by the surface modification.

Single point quantum yield (**Equation 1**) measurements were calculated at 0.1 absorbance and the correlating fluorescence emission for all Qdot samples and quinine sulfate (**Table 1 and 2**). While the Qdots do exhibit a lower QY compared to commercial Qdots (0.4 reported value), they are similar to values reported by Holloway and Yang [13]. In addition, surface modification with NAC increased the QY for both types of Qdots indicating that quantum efficiency can be improved depending on how the Qdots are modified.

3.2 Zeta Potential

Zeta potential measured the electrophoretic mobility of the Qdots in DI water (T**able 3 and 4**). Generally, particles with zeta potentials that are more negative than -30 mV or more positive that +30 mV are considered to be highly stable[44] due to the ability to repel particles and prevent aggregation. The commercial Qdots have reported Zeta potentials ranging from -30 to -50mV, indicating that they are stable colloidal suspensions. The surface modified Qdots exhibit lower Zeta potentials than the bare Qdots due to the presence of carboxylic acids in the ligands. In addition, the tendency for bare Qdots to aggregate is supported by their near-neutral zeta potential, which shows a lacking ability to repel particles.

3.3 Surface Functionality Characterization

Surface functional groups were characterized by H^1 NMR spectroscopy. Bare Qdots are insoluble in both D_2O and DMSO-d6 causing them to aggregate and settle. As a result, H^1 NMR for the residual AOT could not be detected (**Figure 10 and 13**).

The AOT control (**Figure 7**) was still necessary because all of the Qdots have some residual AOT on them. AOT was solubilized in DMSO-d6 for H^1 NMR. The doublet of doublet peak at 3.6ppm corresponds to the chiral proton near the sulfite. The singlet peak around 1.5ppm corresponds to the two chiral protons in the CH groups. The methyl and CH_2 groups are assigned to the multiplets occurring before and after 1ppm respectively. The two doublet of doublet peaks at 2.8 correspond to the protons attached to the carbon surrounded by the oxygens from the ester and sulfite group. The multiplet peak at 3.9 corresponds to the proton atoms positioned near the single bonded oxygen of the ester group.

NAC was solubilized in D_2O (**Figure 8**). The doublet of doublets at 4.5 ppm corresponds to the *alpha* proton. The AB pattern around 2.8 ppm corresponds to the *beta* CH_2. The singlet at 1.9 ppm corresponds to the amide methyl group. The acid, thiol, and amide protons are not visible due to exchange with the deuterated solvent.

Lipoic acid was solubilized in DMSO-d6 (**Figure 9**). H^1 NMR of Lipoic Acid in Dimethyl Sulfoxide-d6. DMSO quintet peak at 2.5 ppm is the reference peak. Singlet at 12 ppm corresponds to the carboxylic acid. The multiplet peak at 3.6 ppm corresponds to the chiral proton. The remaining peaks correspond to the protons positioned on the CH_2 groups.

In order to verify that the surface functional groups corresponded to the appropriate ligand, peaks that were specific to only NAC. NAC coated CdS:Mn/ZnS Qdots (**Figure 11**) showed peaks that corresponded to both the *beta* CH_2 and amide methyl group whereas NAC

coated ZnS:Mn/ZnS (**Figure 14**) showed peaks that corresponded amide methyl group. Since those protons were not detected in the AOT control, NAC conjugation to the Qdot was confirmed.

As for the DHLA conjugation, detecting protons that corresponded to only LA was the confirmatory objective. DHLA coated CdS:Mn/ZnS Qdots (**Figure 12**) showed two distinct peaks that only correspond to the CH_2 groups of the five membered ring (3.2ppm and 2.4ppm). DHLA coated ZnS:Mn/ZnS Qdots (**Figure 15**) showed the same two peaks as the DHLA coated CdS:Mn/Zns Qdots in addition to a peak corresponding to the CH_2 located next to the carboxylic acid. The absence of proton peaks below 2.2ppm indicates the absence of both AOT and LA related protons from the carbon chain.

3.4 High Resolution Transmission Electron Microscopy

Energy dispersive X-Ray spectroscopy confirmed the presence of Cd, Mn, Zn, and S in the CdS:Mn/ ZnS Qdots (**Figure 16 and 20**), and Zn, Mn, and S in the ZnS:Mn/ZnS Qdots (**Figure 24 and 28**). The copper and carbon signals are due to the carbon film on the copper TEM grid. Low resolution images of each coated Qdot were captured to visualize particle dispersion (**Figure 17, 21, 25, 29**) and high resolution images were captured to visualize the lattice planes, measure lattice spacing, and visualize the crystallinity using selected area electron diffraction (SAED). Electron rich material, seen as dark contrast, corresponds to surface modified CdS:Mn/ZnS Qdots (**Figure 18 and 22**) and ZnS:Mn/ZnS Qdots (**Figure 26 and 30**). Single particles are further magnified in the inset to better observe the lattice planes of the crystalline particles.

SAED of the CdS:Mn/ZnS Qdots (**Figure 19 and 23**) show bright distinct rings indicating the crystalline particles. Three rings (inner, middle, outer) were detected for each Qdot

sample measuring 3.15Å, 1.94 Å, and 1.63 Å in diameter respectively. Lattice spacing references indicated that the 3.15Å corresponds to the CdS semiconductor core and the 1.94 Å corresponds to the ZnS semiconductor shell. The 1.63 Å spacing is not specific enough to have only one reference.

SAED of the ZnS:Mn/ZnS Qdots (**Figure 27 and 31**) show very bright distinct rings that indicate the crystallinity of the particles. The spacing for the three rings (inner, middle, and outer) were 3.09 Å, 1.90 Å, and 1.59 Å in diameter respectively. Lattice spacing references indicated that both the 3.09 Å and 1.90 Å lattice spacing correlated to ZnS, however the 1.59 Å was not specific enough to attribute to a specific reference.

3.5 Compromised Quantum Dots

Fluorescence quenching using 30μL of 6N HCl was seen for all Qdot samples (**Figure 32 and 33**). The complete quenching of the ~590nm peak intensity indicated that the integrity of the Mn dopant core had been compromised. HCl compromises Qdots disassociating the components into metal salts ($CdCl_2$, $ZnCl_2$ and MnCl2). Even after restoring the pH with 6M NaOH, the fluorescence did not restore, which indicates an irreversible quenching effect from HCl.

3.6 Bacterial Toxicity

The surface agents of the Qdots (AOT, NAC and DHLA) all affect bacteria differently. AOT and NAC are known antimicrobials in high concentrations, NAC and DHLA are known antioxidants, and DHLA has not been shown to have antimicrobial properties. Interestingly, the residual amount of AOT that is present on the Qdots is not enough to completely inhibit the growth of *E. coli* (**Figure 38),** even though AOT is commonly used as a pesticide. High concentrations of LA inhibit *E. coli* growth (**Figure 40**). NAC has shown to have antimicrobial properties, which explains why it is inhibiting *E. coli* growth (**Figure 39**). The cadmium salts

completely inhibit *E. coli* growth compared to the zinc salts which are less inhibitory at the same concentration (**Figure 41**). Looking at actual toxicity (**Figure 48**), only AOT and DHLA exhibited the least toxic affect on *E. coli.*

Compared to the untreated control, high concentrations of commercial Qdots exhibited an inhibitory effect on *E. coli* growth and turbidity (**Figure 34 and 37**). Toxicity results revealed that the commercial Qdots were not inhibiting *E.coli* growth and viability as the total colony counts were almost identical to the growth control (**Figure 47**). Differences in the optical density and turbidity can be attributed to the effect of the Qdots in LB broth. The CdS:Mn/ZnS and ZnS:Mn/ZnS Qdots exhibited similar results as the commercial Qdots indicating that the optical density differences are due to the behavior of the bare Qdots in LB broth (**Figure 35, 36, 42, and 45**). Given that bare Qdots are insoluble in water, they are likely to aggregate in LB broth as well. Unlike the commercial Qdots, bare Qdots did exhibit a toxic affect on *E. coli* (**Figure 49 and 51**) which is due to lack of additional coating that commercial Qdots are equipped with.

The surface modified CdS:Mn/ZnS Qdots exhibited more of an inhibitory affect on the growth of *E. coli* than the surface modified ZnS:Mn/ZnS (**Figure 35 and 36**). Judging by the bactericidal assays (**Figure 49 and 51**) the inhibition from the surface modified CdS:Mn/ZnS Qdots is not due to the behavior of the Qdots in LB broth, but moreso a toxic effect on the bacteria. Since NAC and DHLA increase the bioavailability of the Qdots it is likely that the Qdots are physically interacting with *E. coli*. While the surface modified ZnS:Mn/ZnS Qdots also exhibit deviations in *E. coli* growth compared to the untreated control, only the NAC coated Qdot is inhibiting (**Figure 36**). In addition, compared to the CdS:Mn/ZnS Qdots, the ZnS:Mn/ZnS Qdots are not as toxic (**Figure 49 and 51**) .

Looking at just the compromised Qdots, it is clear that the ZnS:Mn./ZnS Qdots are less toxic than both commercial and CdS:Mn/ZnS Qdots (**Figure 49 and 51**). In addition, surface modification with NAC and DHLA minimized the toxicity from compromised cadmium Qdots compared to compromised commercial Qdots (**Figure 50**) indicating that the presence of antioxidants may play a role in reducing cadmium related toxicity.

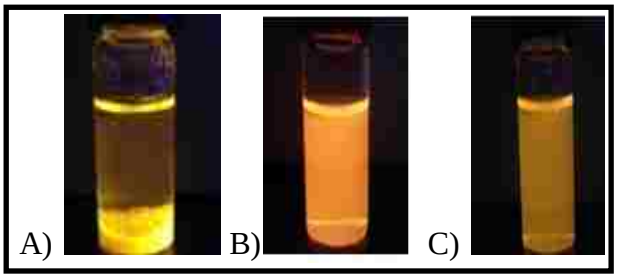

Figure 1- Fluorescence Emission of CdS:Mn/ZnS Qdots by handheld UV light source

A) Bare, B) NAC coated, C) DHLA coated

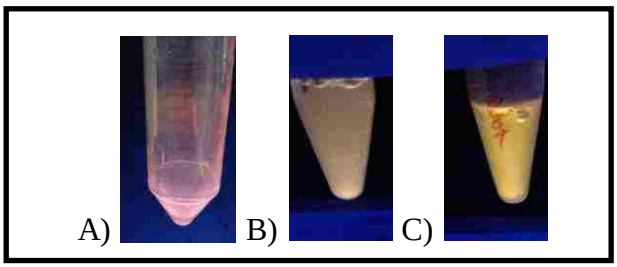

Figure 2- Fluorescence Emission of ZnS:Mn/ZnS Qdots by handheld UV light source

Bare, B) NAC coated, C) DHLA coated

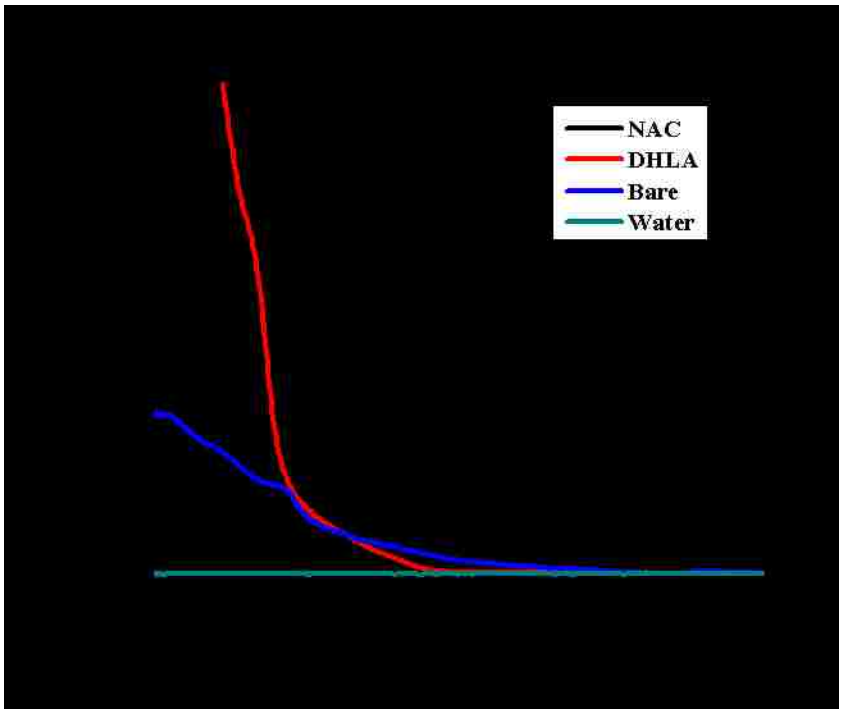

Figure 3- UV-Visible spectroscopy of coated and uncoated CdS:Mn/ZnS Qdots in DI water

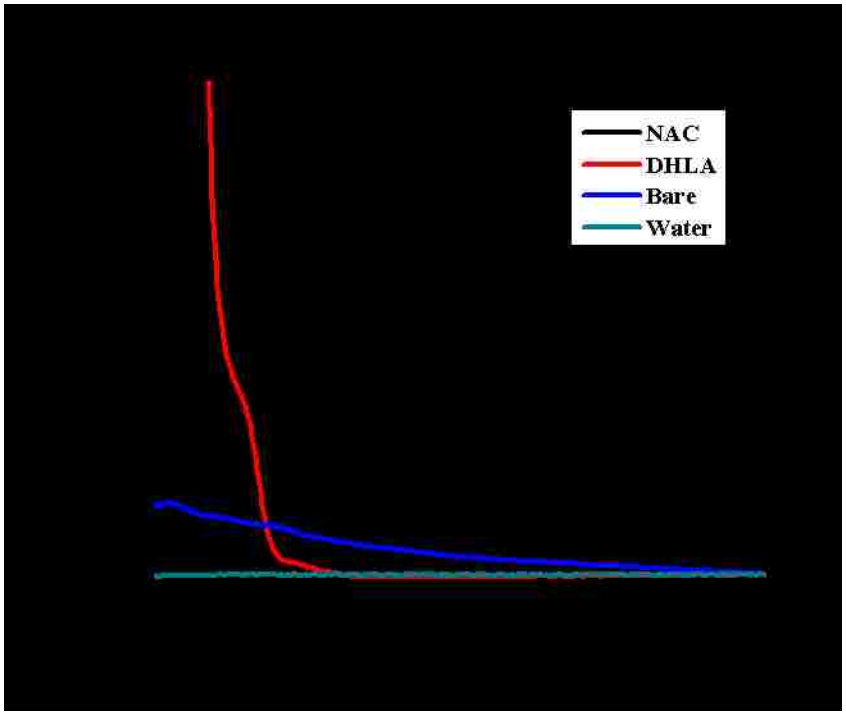

Figure 4- UV-Visible spectroscopy of coated and uncoated ZnS:Mn/ZnS Qdots in DI water

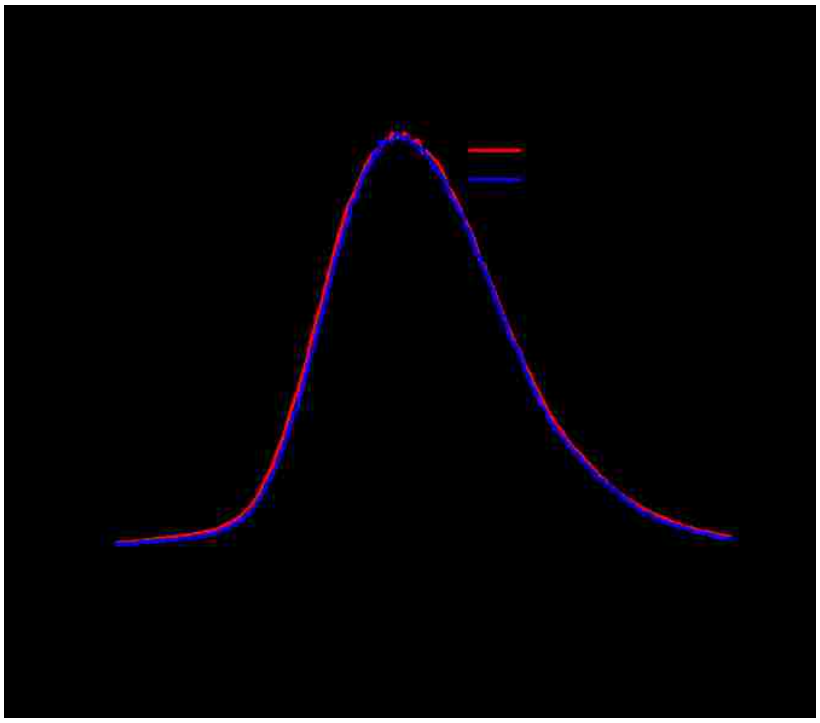

Figure 5- Normalized fluorescence spectroscopy of coated and uncoated CdS:Mn/ZnS Qdots in DI water. Excitation λ: 375nm

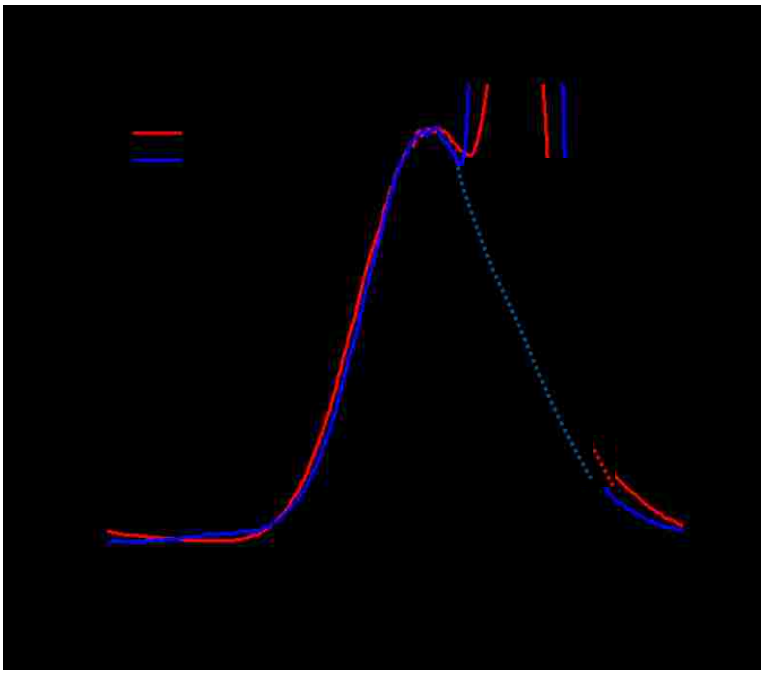

Figure 6 – Normalized fluorescence spectroscopy of coated and uncoated ZnS:Mn/ZnS Qdots in DI water. Excitation λ: 308nm

Table 1- Quantum Yield calculations for coated and uncoated CdS:Mn/ZnS Qdots.

Reference standard is Quinine Sulfate in 0.1M H_2SO4

Sample	**Φ_f**
Bare CdS:Mn/ZnS	0.10
NAC coated	0.16
DHLA Coated	0.15

Table 2- Quantum Yield calculations for coated and uncoated ZnS:Mn/ZnS Qdots.

Reference standard is Quinine Sulfate in 0.1M H2SO4

Sample	**Φ_f**
Bare ZnS:Mn/ZnS	0.13
NAC coated	0.16
DHLA Coated	0.10

$$\Phi_X = \Phi_R \frac{I}{I_R} \frac{OD_R}{OD} \frac{n2}{n2_R} \quad (1)$$

Table 3- Zeta Potential measurements of coated and uncoated CdS:Mn/ZnS

CdS:Mn/ZnS	**Zeta Potential (mV)**
Bare	-9 +/- 0.5
NAC Coated	-47 +/- 6
DHLA Coated	-40 +/- 6

Table 4- Zeta Potential measurements of coated and uncoated ZnS:Mn/ZnS

ZnS:Mn/ZnS	**Zeta Potential (mV)**
Bare	-2 +/- 0.5
NAC Coated	-48 +/- 8
DHLA Coated	-51 +/- 5

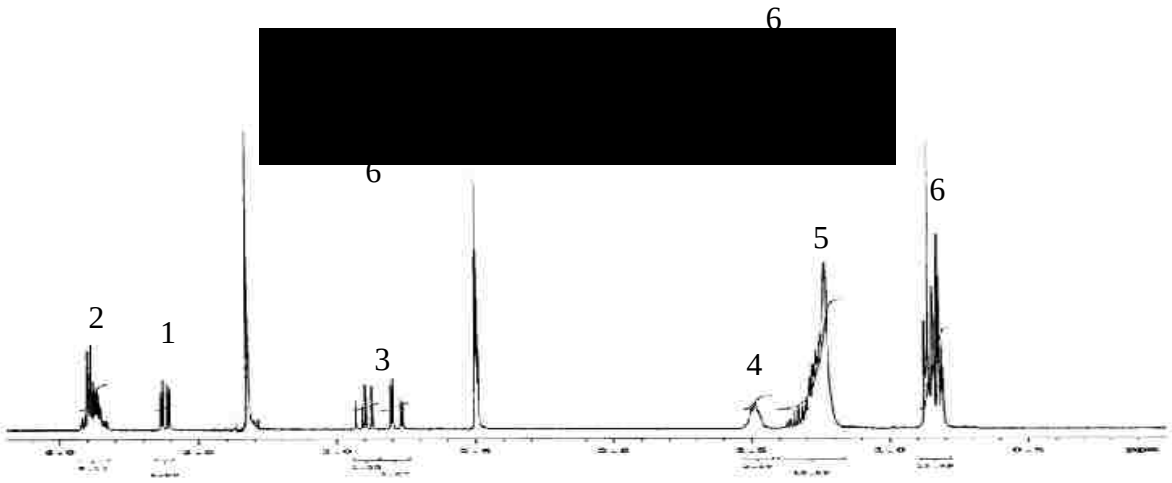

Figure 7- Nuclear Magnetic Resonance Spectroscopy of AOT

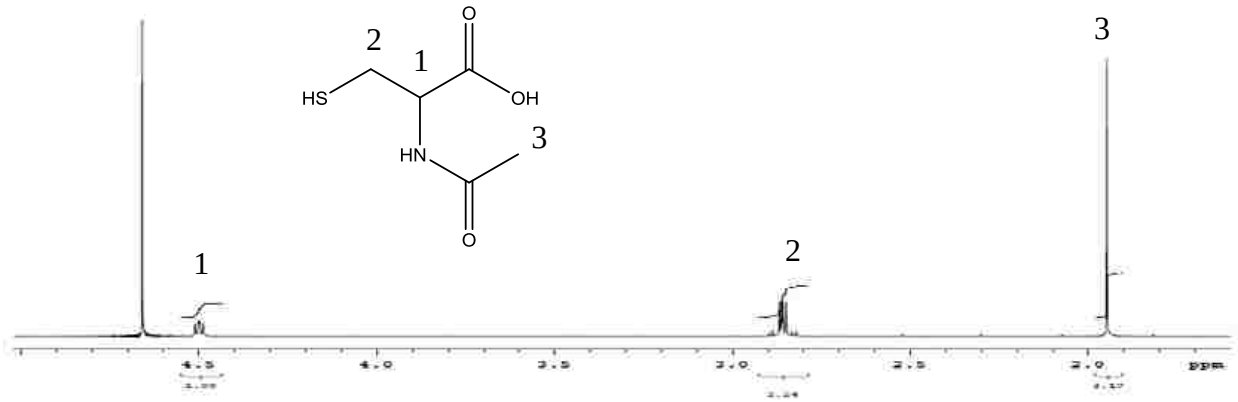

Figure 8- Nuclear Magnetic Resonance Spectroscopy of N-acetylcysteine

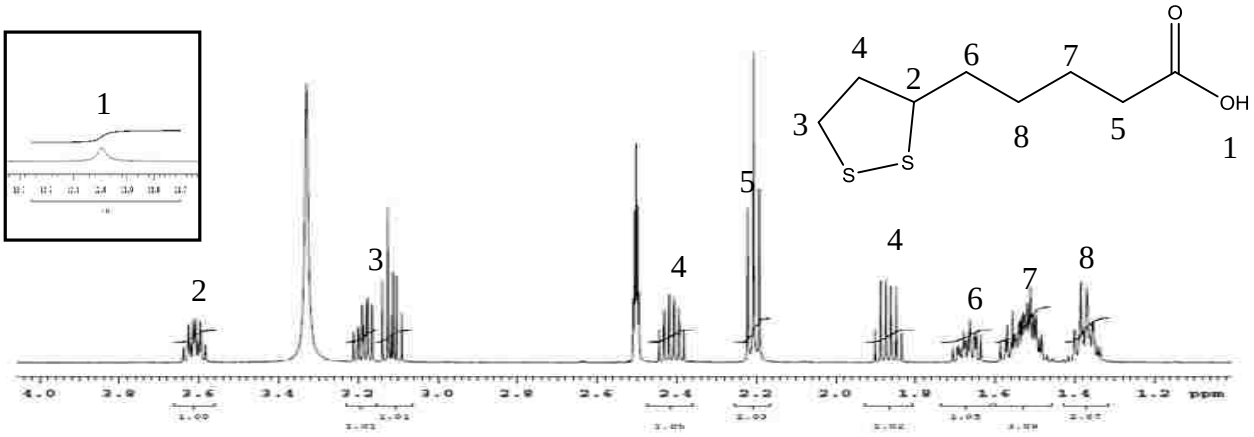

Figure 9- Nuclear Magnetic Resonance Spectroscopy of Lipoic Acid

Figure 10- Nuclear Magnetic Resonance Spectroscopy of bare CdS:Mn/ZnS Qdots

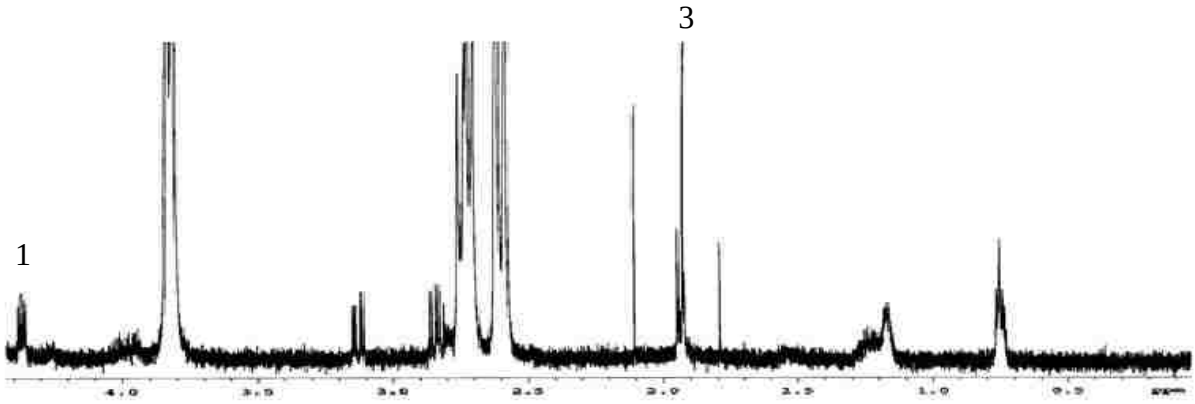

Figure 11- Nuclear Magnetic Resonance Spectroscopy of NAC coated CdS:Mn/ZnS Qdots

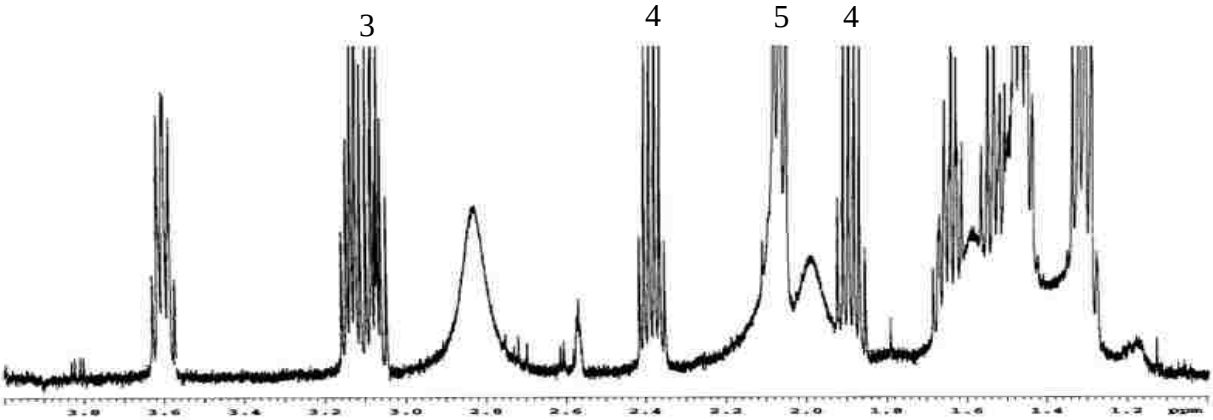

Figure 12- Nuclear Magnetic Resonance Spectroscopy of DHLA coated CdS:Mn/ZnS dots

Figure 13- Nuclear Magnetic Resonance Spectroscopy of bare ZnS:Mn/ZnS Qdots

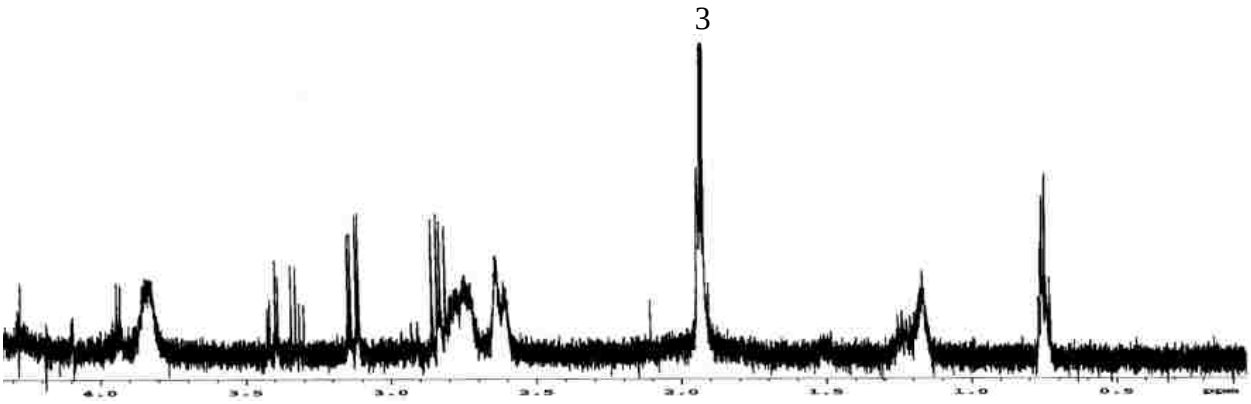

Figure 14- Nuclear Magnetic Resonance Spectroscopy of NAC coated ZnS:Mn/ZnS Qdots

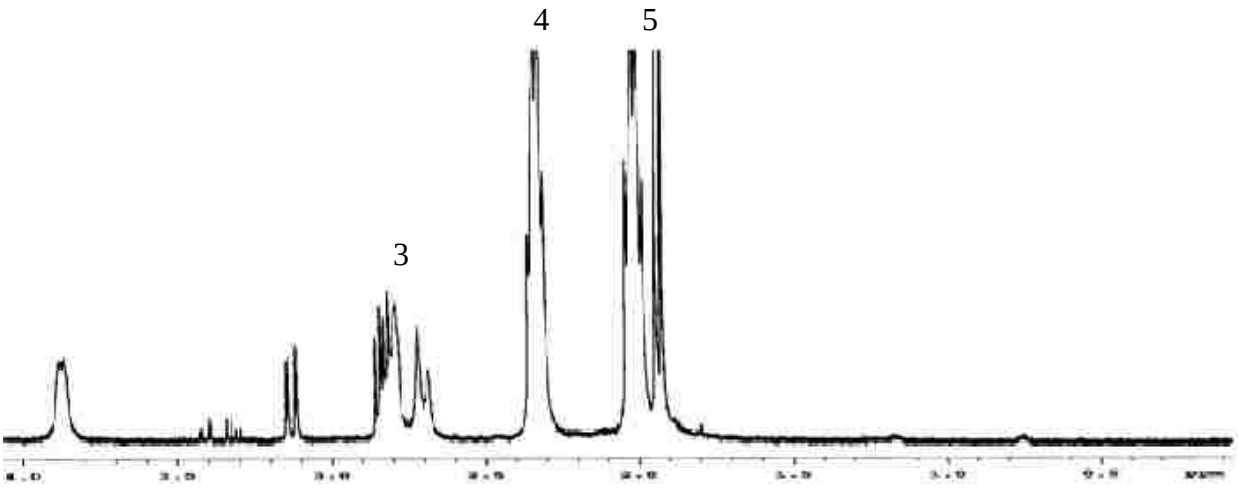

Figure 15- Nuclear Magnetic Resonance Spectroscopy of DHLA coated ZnS:Mn/ZnS Qdots

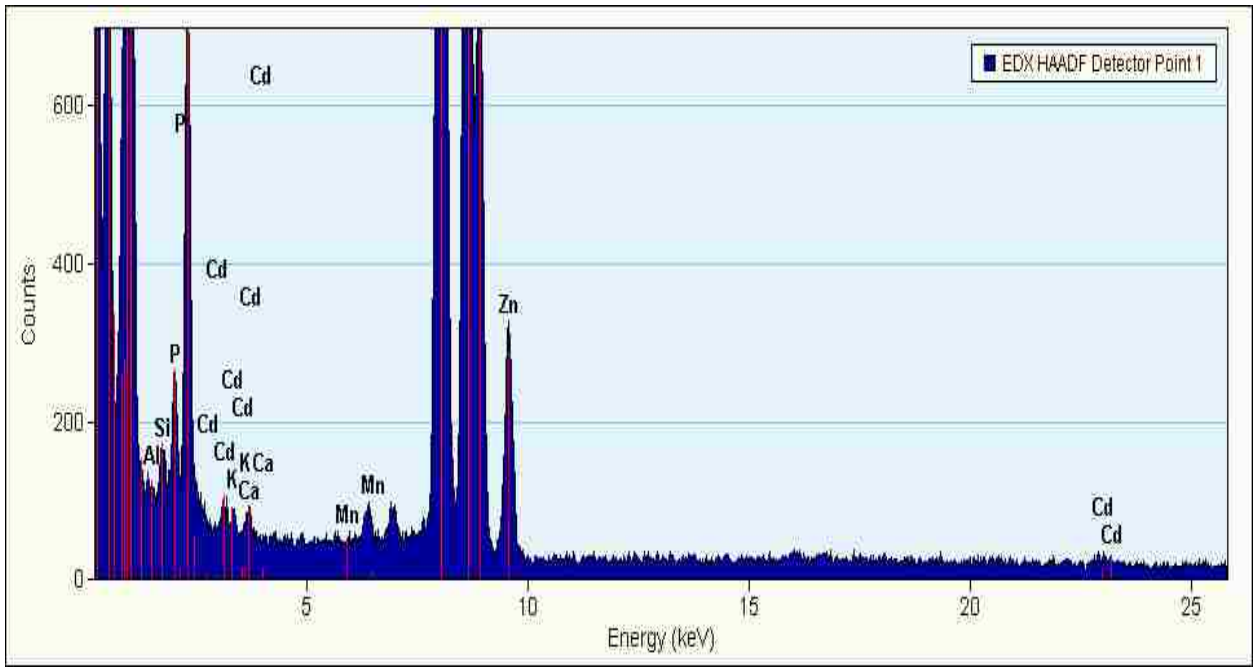

Figure 16- Energy-dispersive X-ray spectroscopy (EDX) for elemental analysis of NAC coated CdS:Mn/ZnS Qdots during HR-TEM

A)

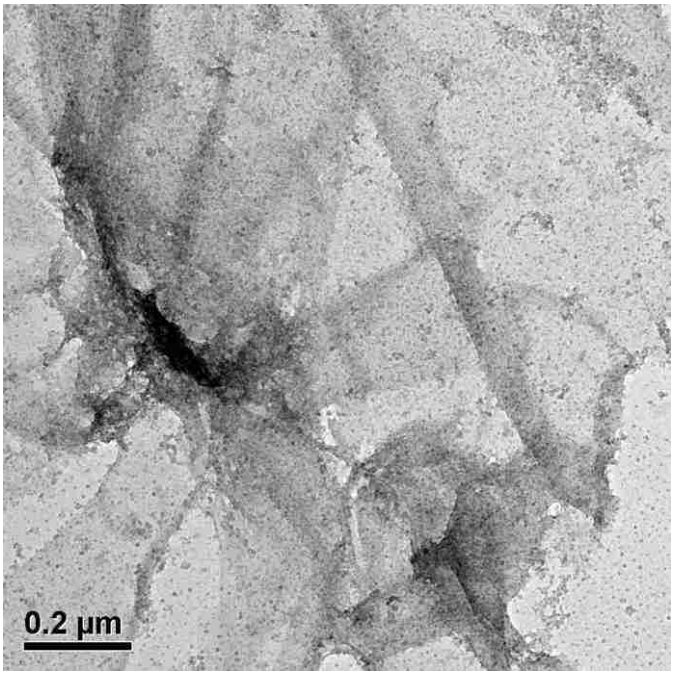

B)

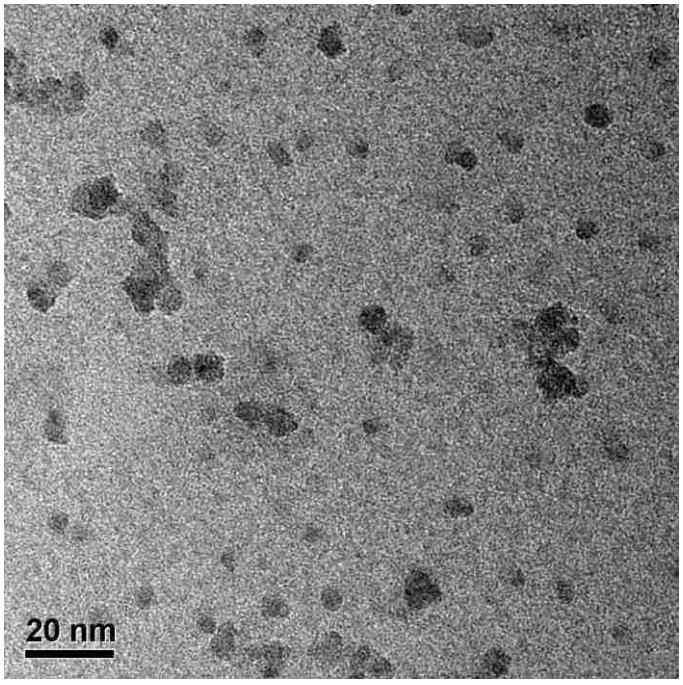

Figure 17-HR-TEM (low mag) image of NAC coated CdS:Mn/ZnS Qdots with scattered dark contrast confirming the presence of electron-rich material

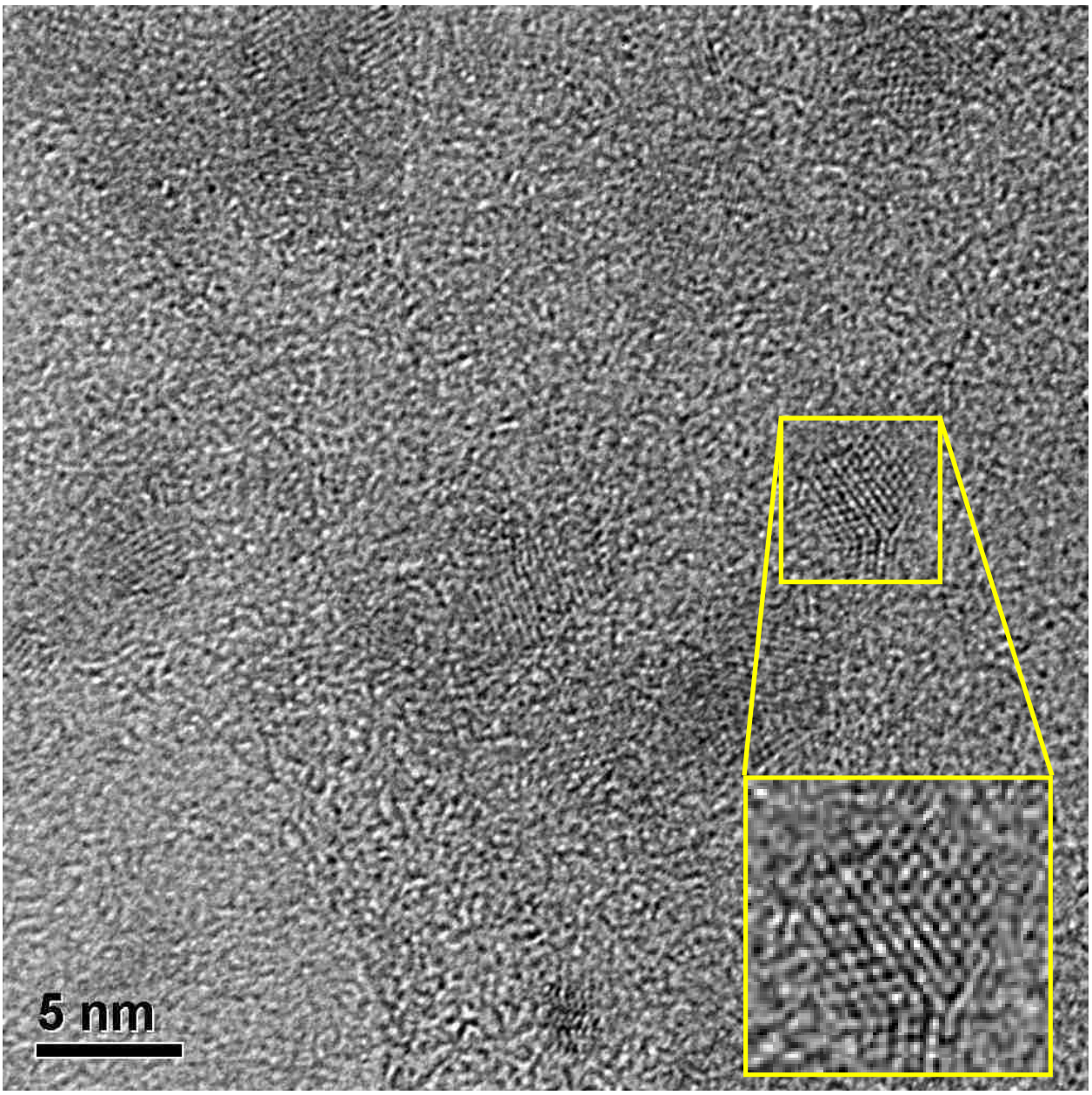

Figure 18- HR-TEM (high mag) image of NAC coated CdS:Mn/ZnS Qdots with scattered dark contrast confirming presence of electron-rich material

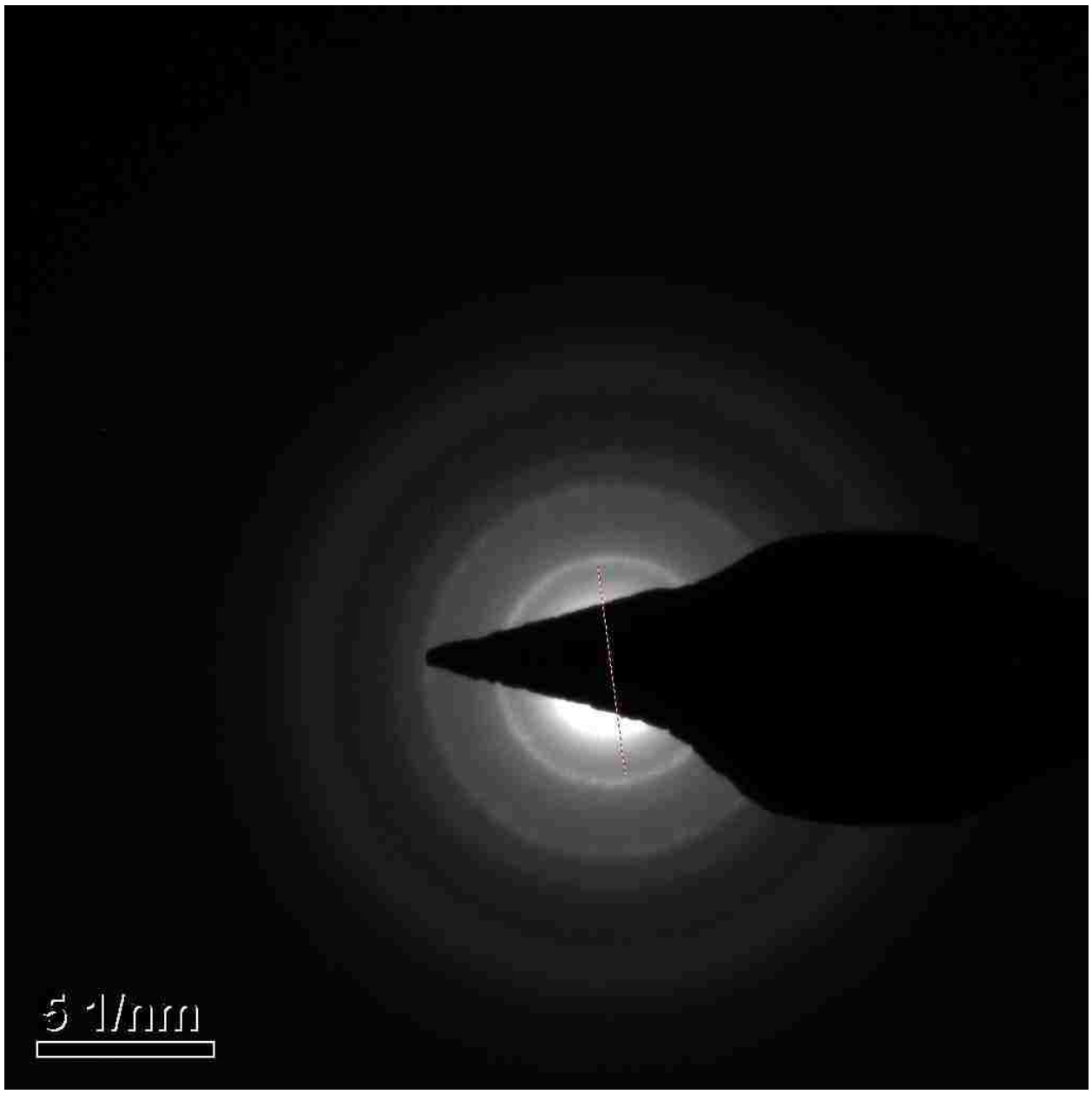

Figure 19- Selected area electron diffraction (SAED) image during HR-TEM of NAC coated CdS:Mn/ZnS Qdots showing the crystallinity.

Lattice spacings 3.15Å, 1.94 Å, and 1.63 Å

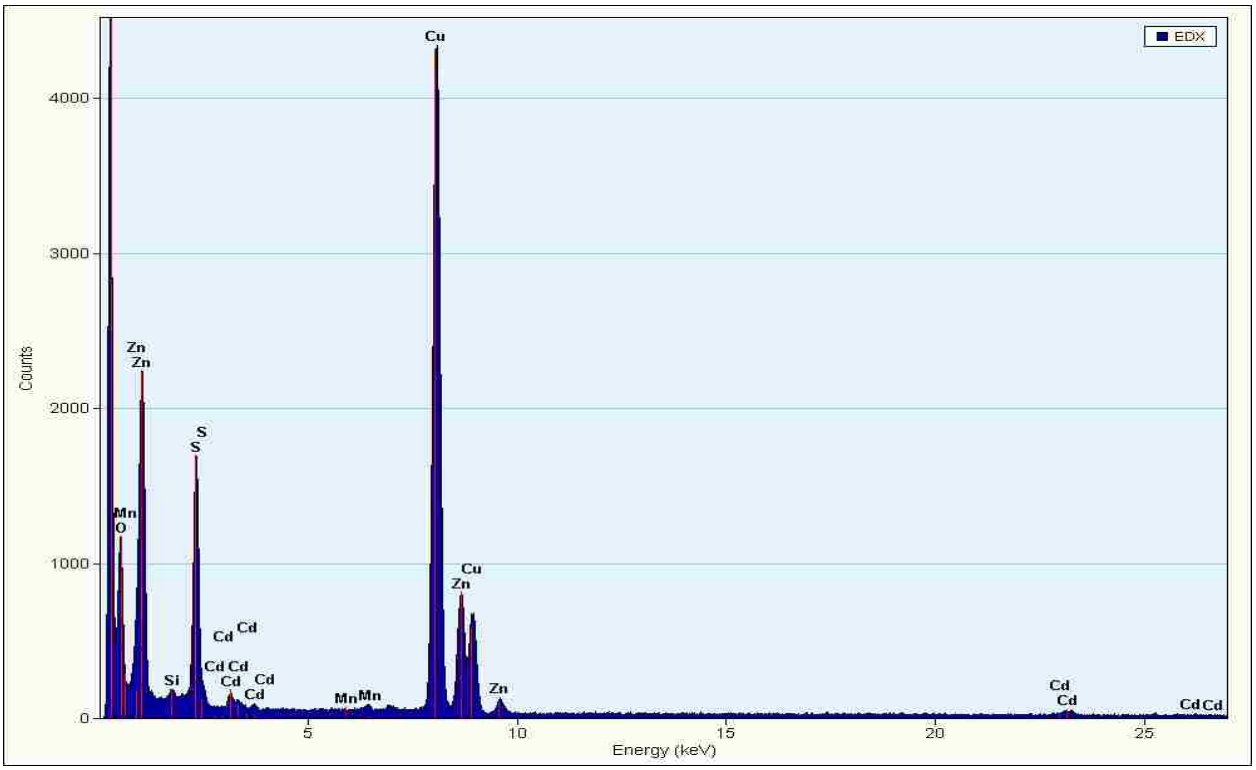

Figure 20- Energy-dispersive X-ray spectroscopy (EDX) for elemental analysis of DHLA coated CdS:Mn/ZnS Qdots during HR-TEM

A) 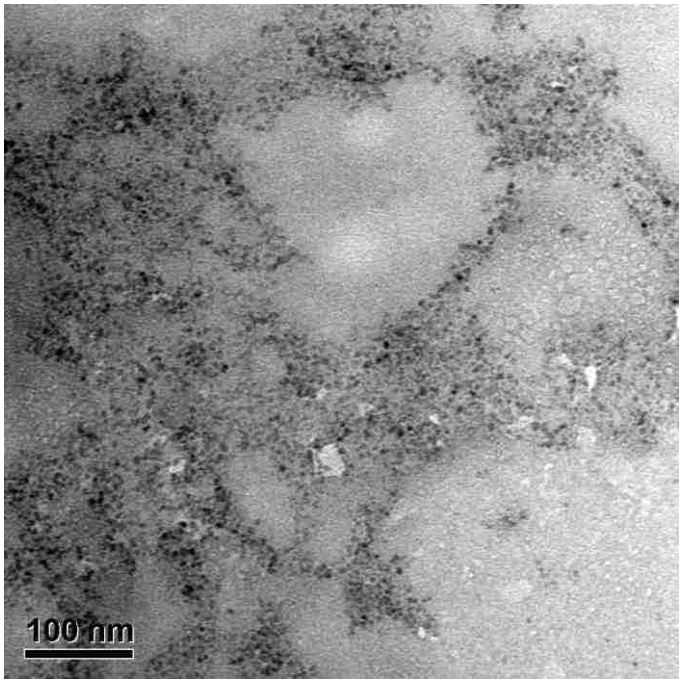

B) 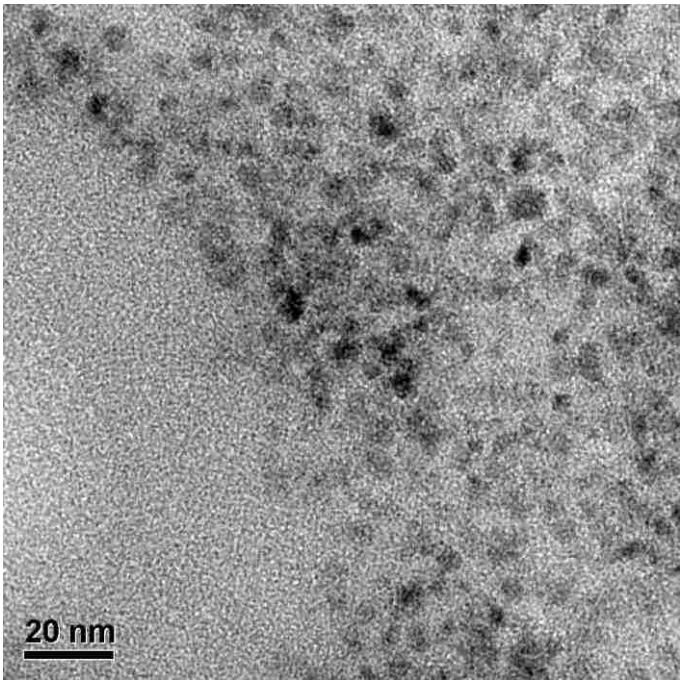

Figure 21-HR-TEM (low mag) image of DHLA coated CdS:Mn/ZnS Qdots with scattered dark contrast confirming presence of electron-rich material

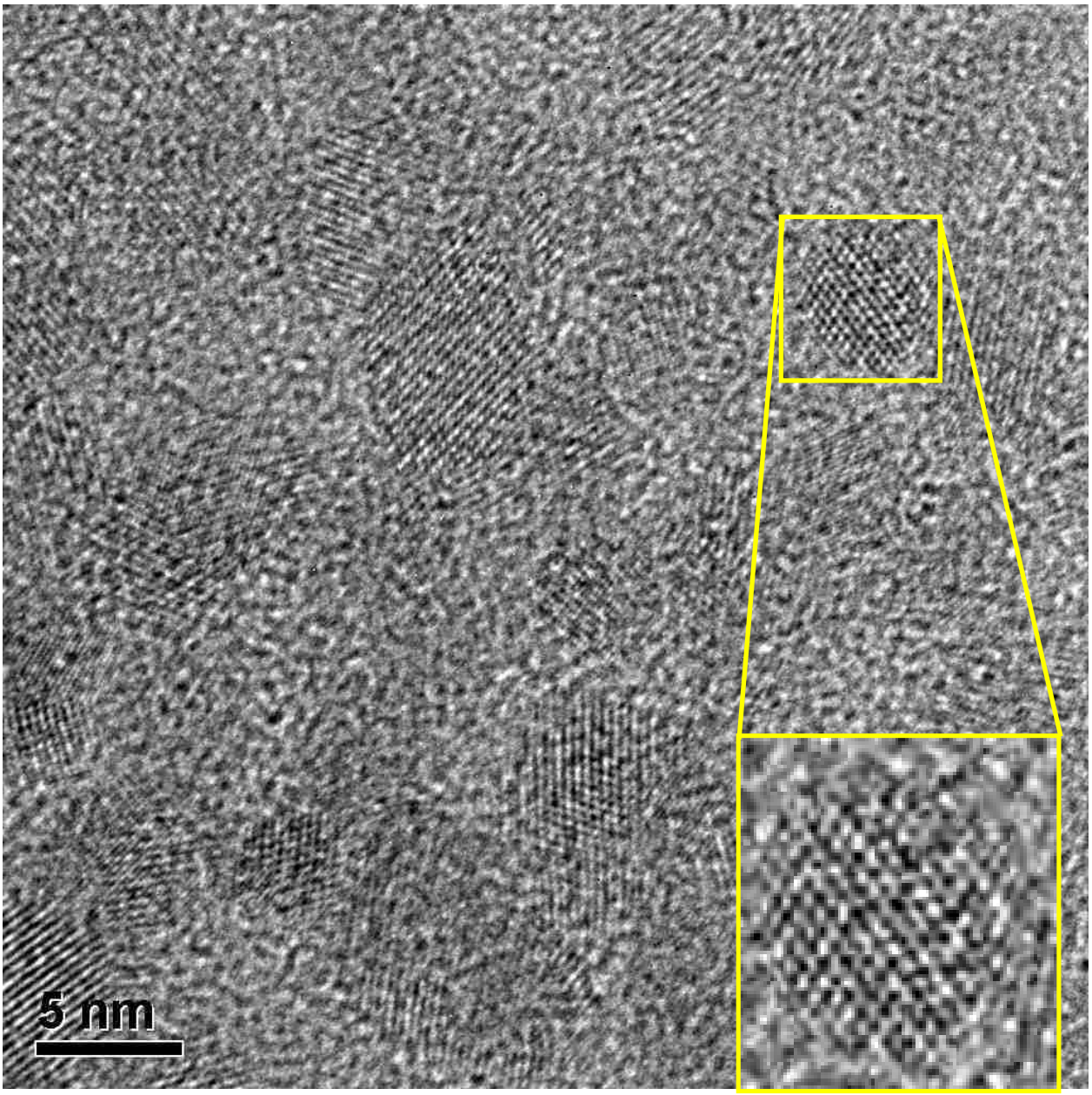

Figure 22- HR-TEM (high mag) image of DHLA coated CdS:Mn/ZnS Qdots with scattered dark contrast confirming presence of electron-rich material

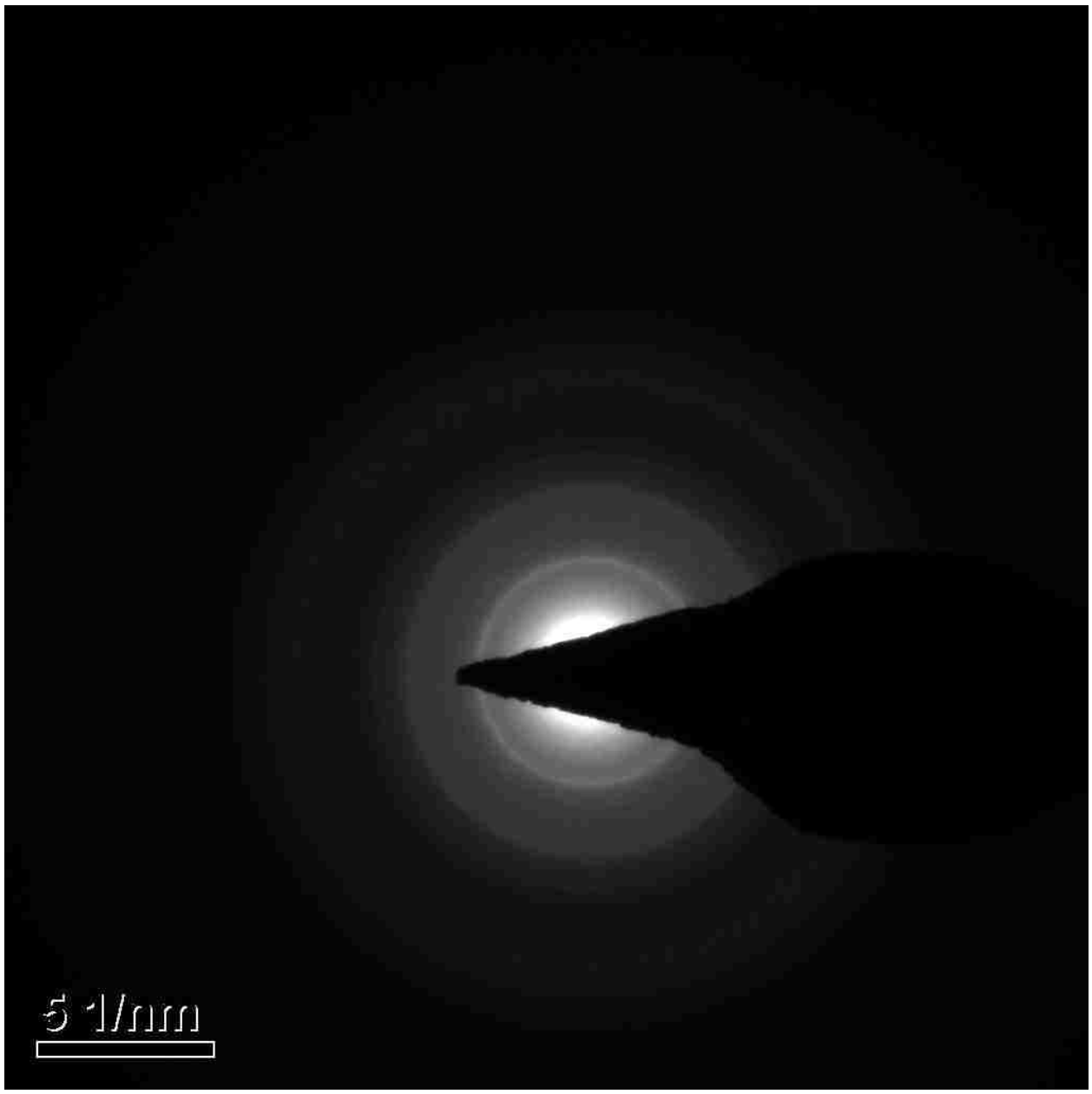

Figure 23- Selected area electron diffraction (SAED) image during HR-TEM of DHLA coated CdS:Mn/ZnS Qdots showing the crystallinity

Lattice spacings 3.15Å, 1.94 Å, and 1.63 Å

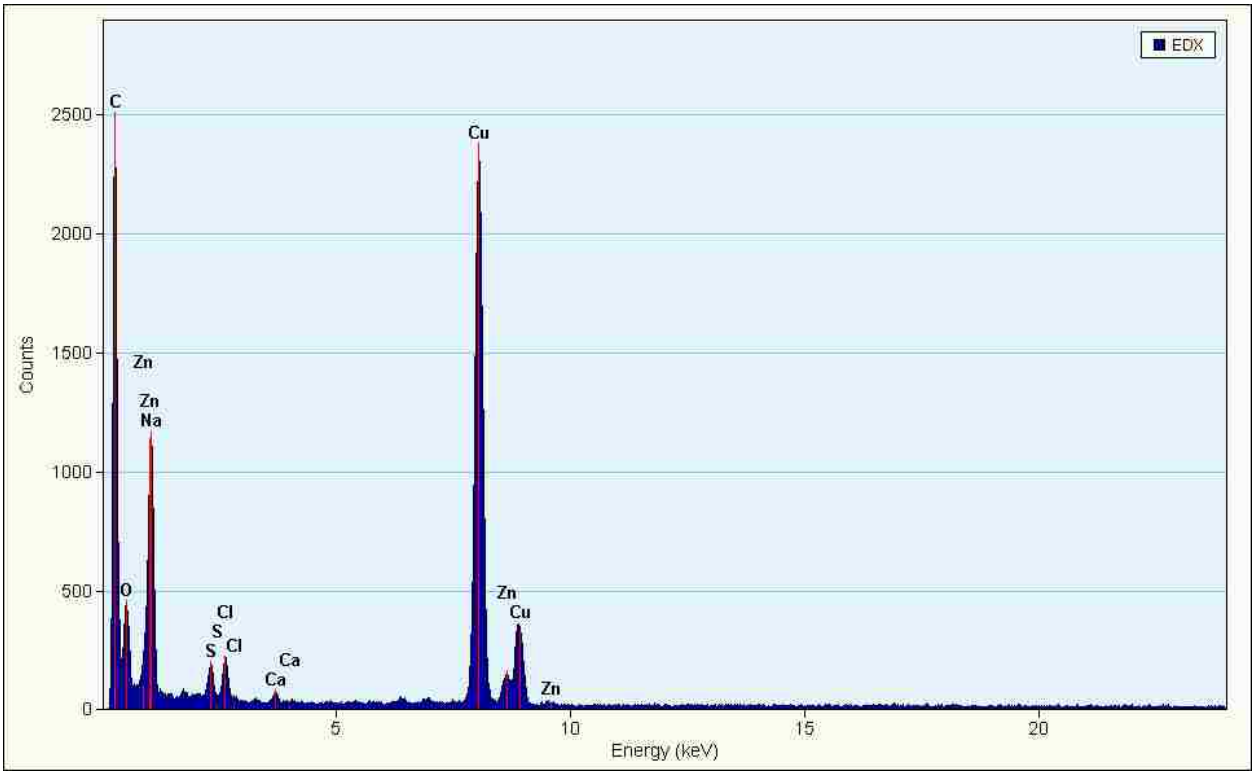

Figure 24- Energy-dispersive X-ray spectroscopy (EDX) for elemental analysis of NAC coated ZnS:Mn/ZnS Qdots during HR-TEM

A)

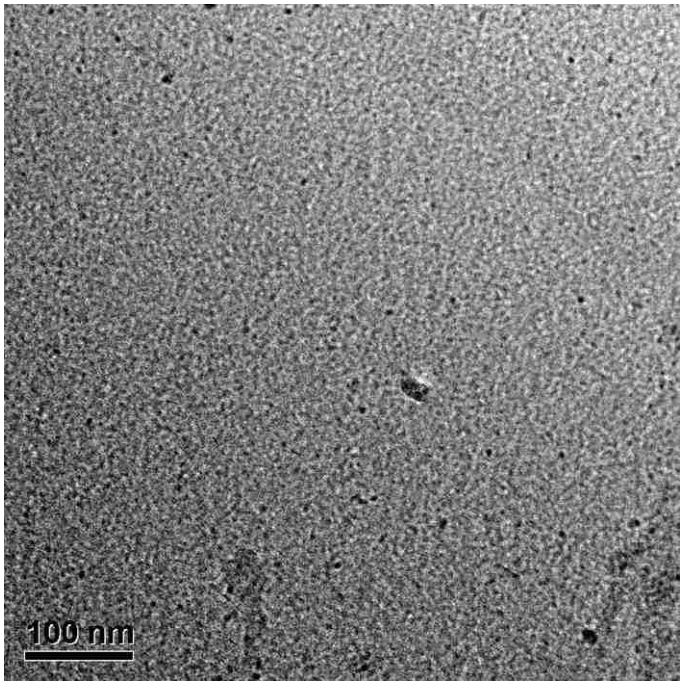

B)

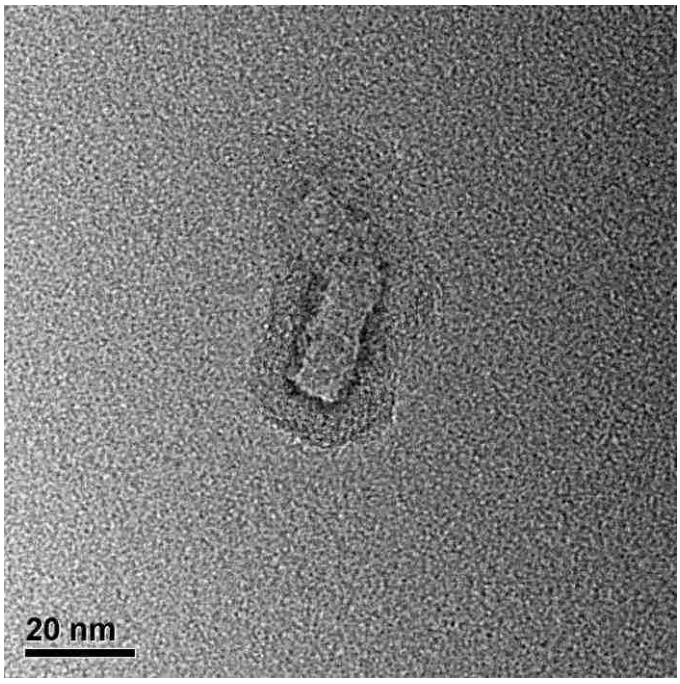

Figure 25-HR-TEM (low mag) image of NAC coated ZnS:Mn/ZnS Qdots with scattered dark contrast confirming presence of electron-rich material

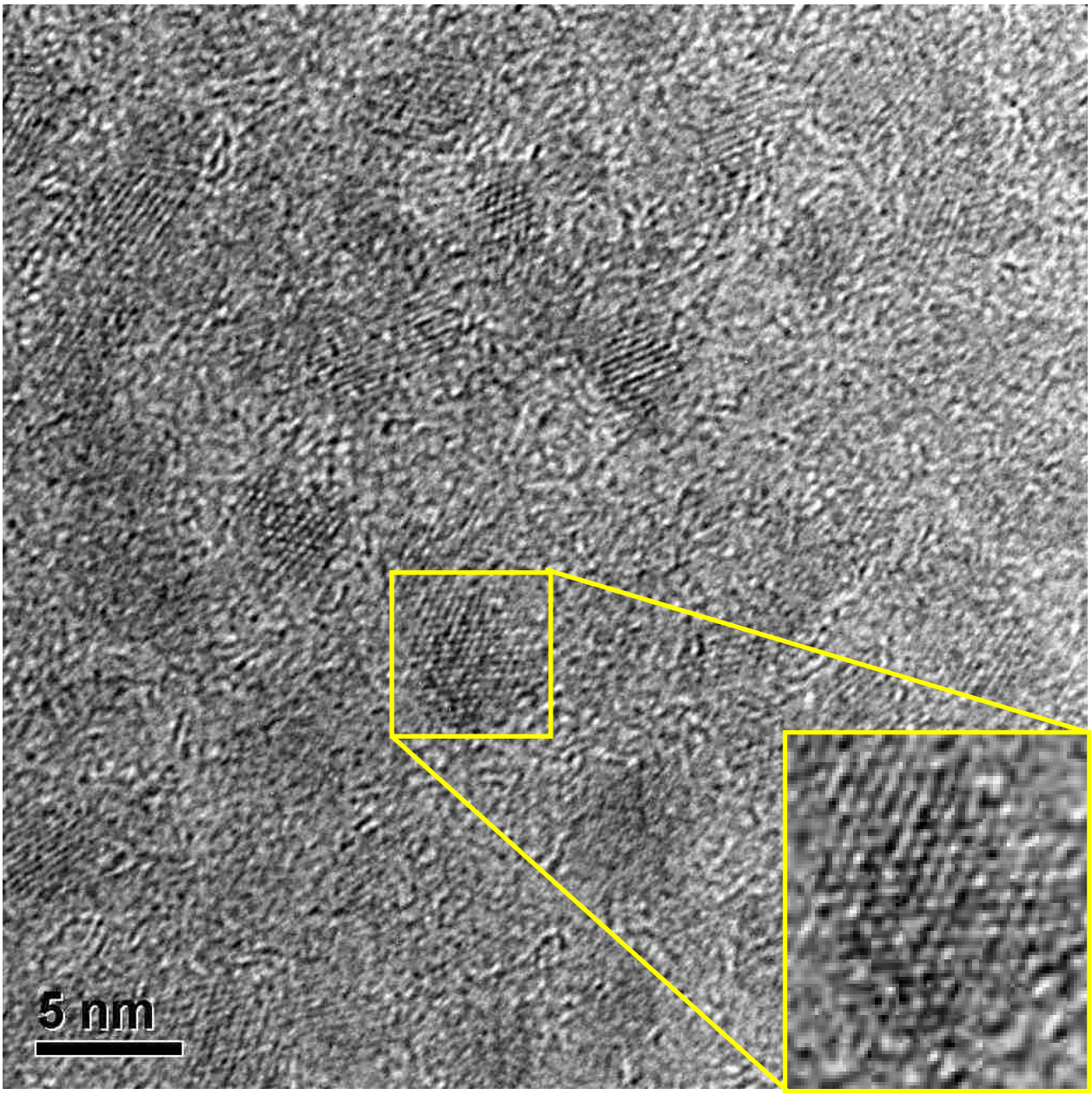

Figure 26- HR-TEM (high mag) image of NAC coated ZnS:Mn/ZnS Qdots with scattered dark contrast confirming presence of electron-rich material

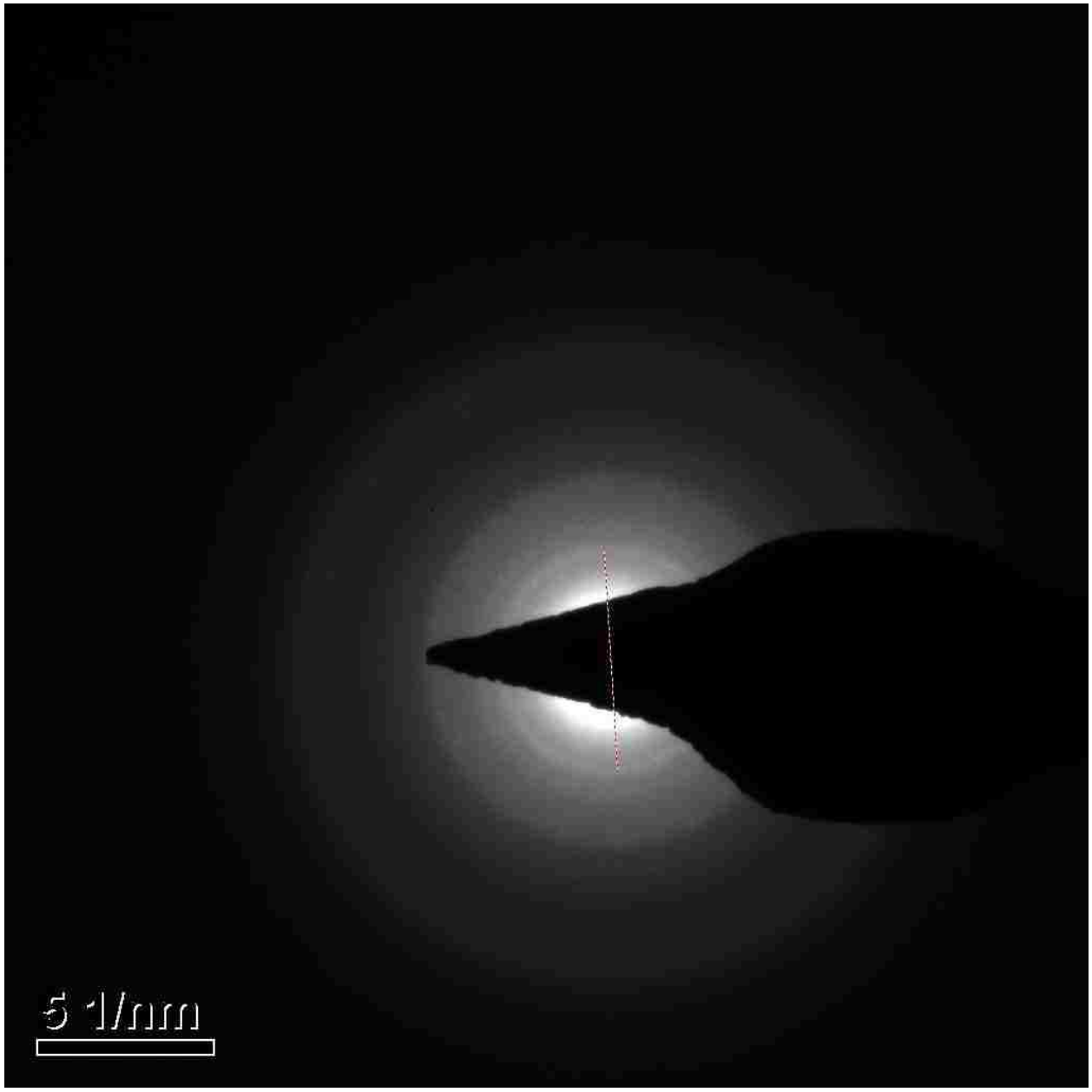

Figure 27- Selected area electron diffraction (SAED) image during HR-TEM of NAC coated ZnS:Mn/ZnS Qdots showing the crystallinity

Lattice spacings ~3.09 Å, ~1.90 Å, and ~1.59 Å

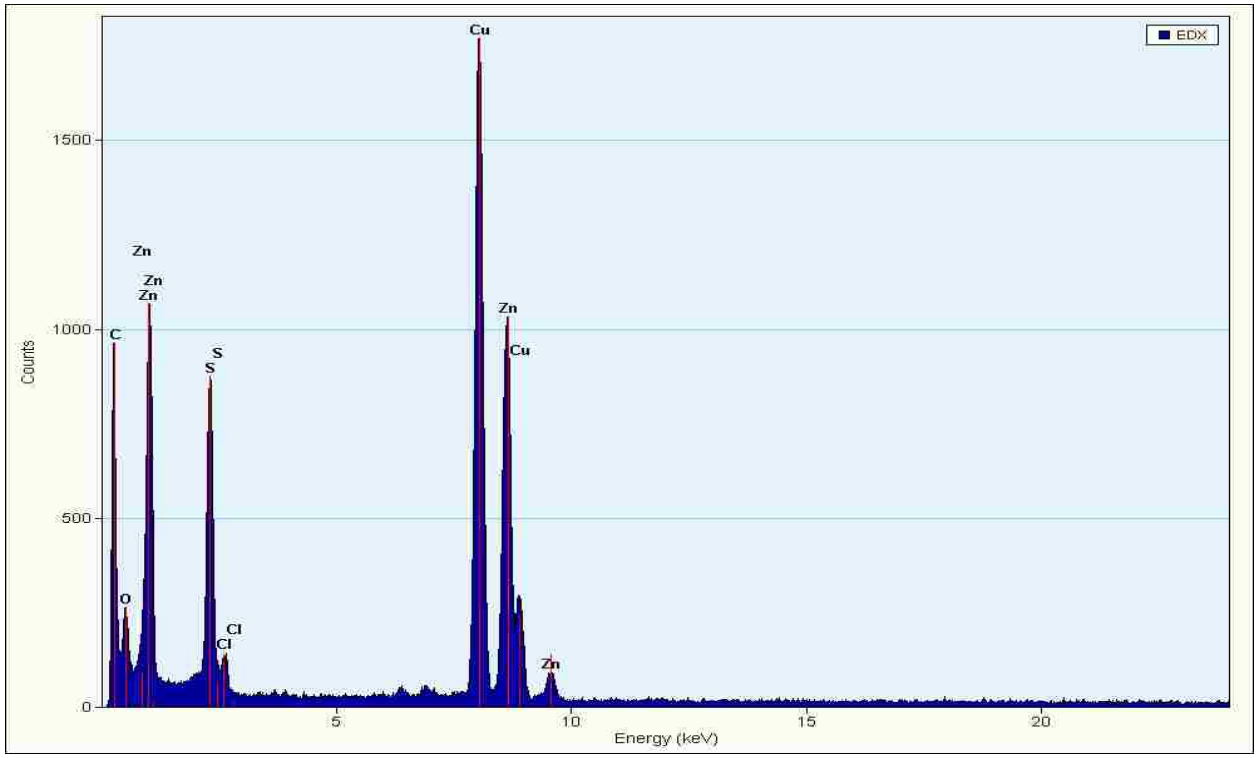

Figure 28- Energy-dispersive X-ray spectroscopy (EDX) for elemental analysis of DHLA coated ZnS:Mn/ZnS Qdots during HR-TEM

A)

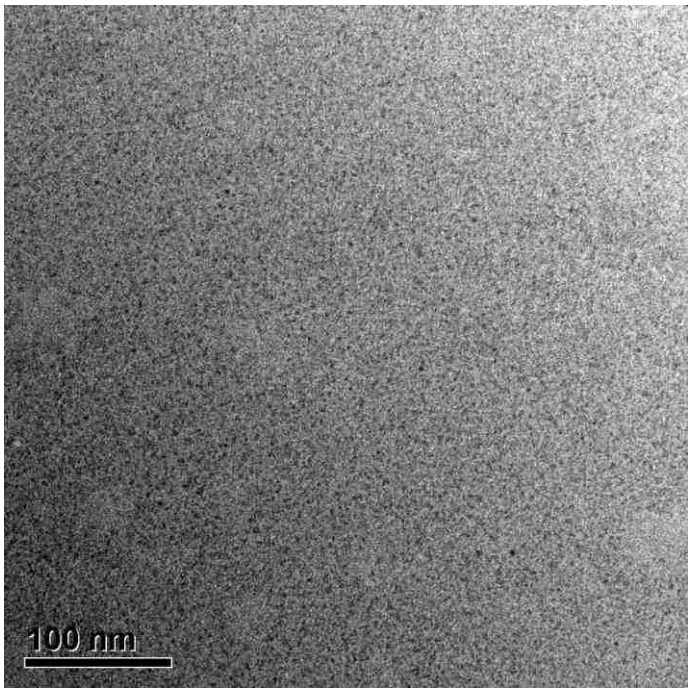

B)

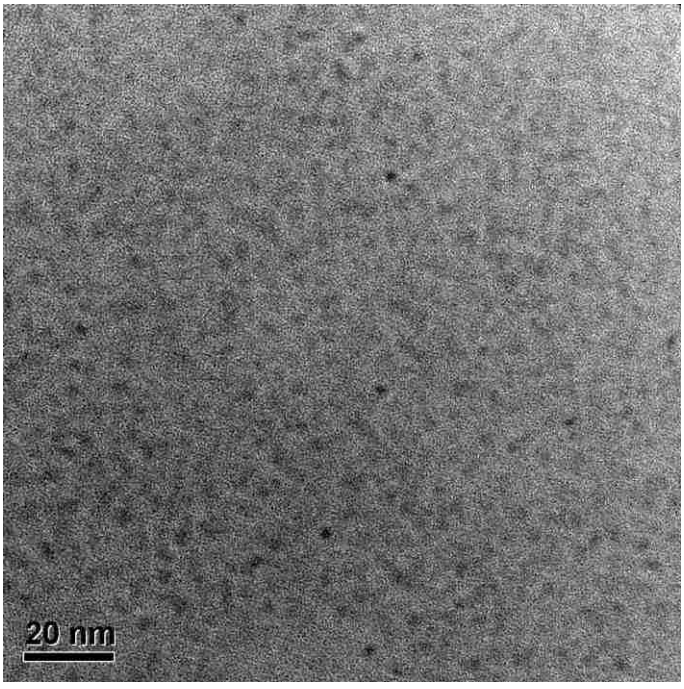

Figure 29-HR-TEM (low mag) image of DHLA coated ZnS:Mn/ZnS Qdots with scattered dark contrast confirming presence of electron-rich material

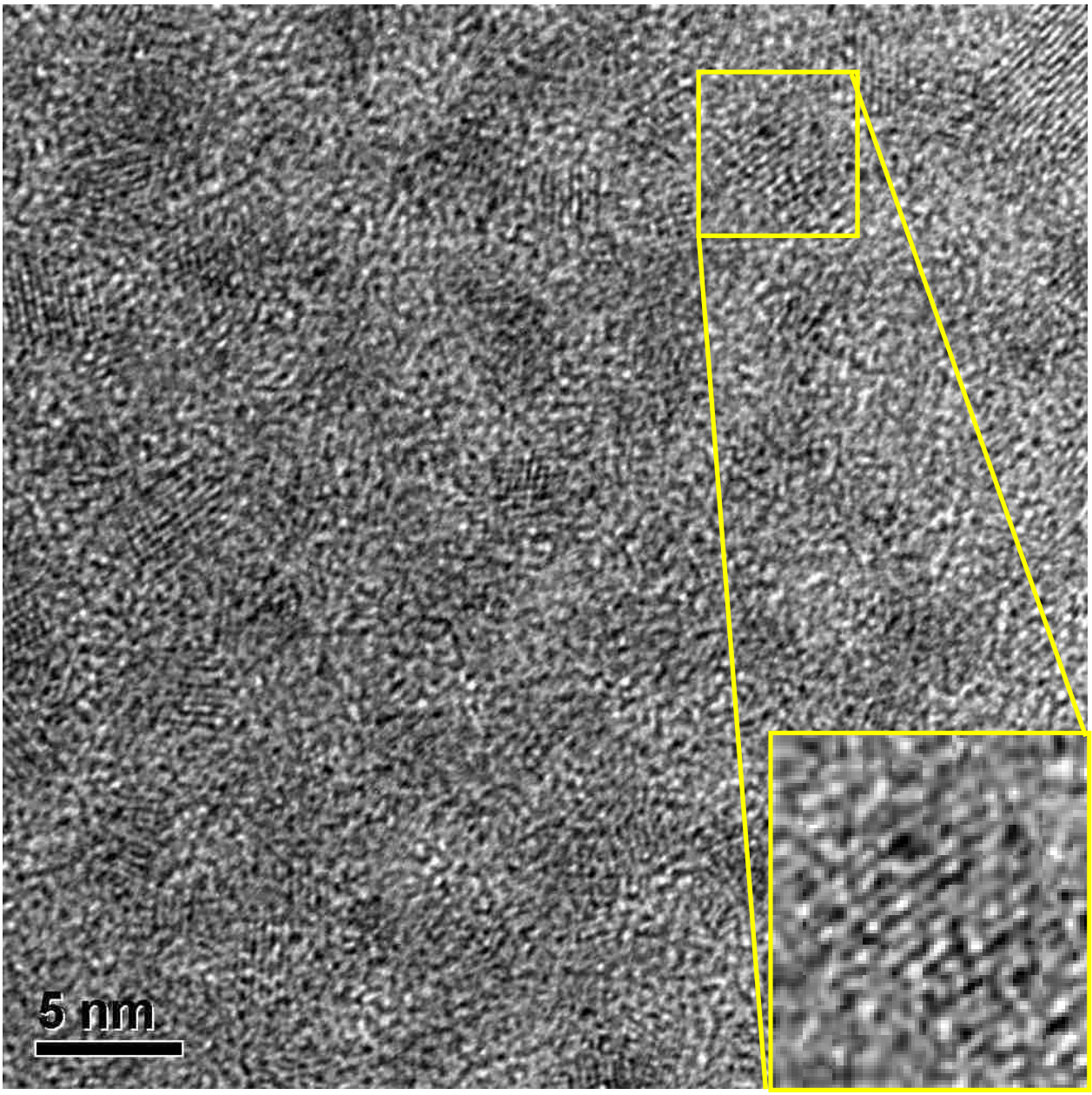

Figure 30- HR-TEM (high mag) image of DHLA coated ZnS:Mn/ZnS Qdots with scattered dark contrast confirming presence of electron-rich material

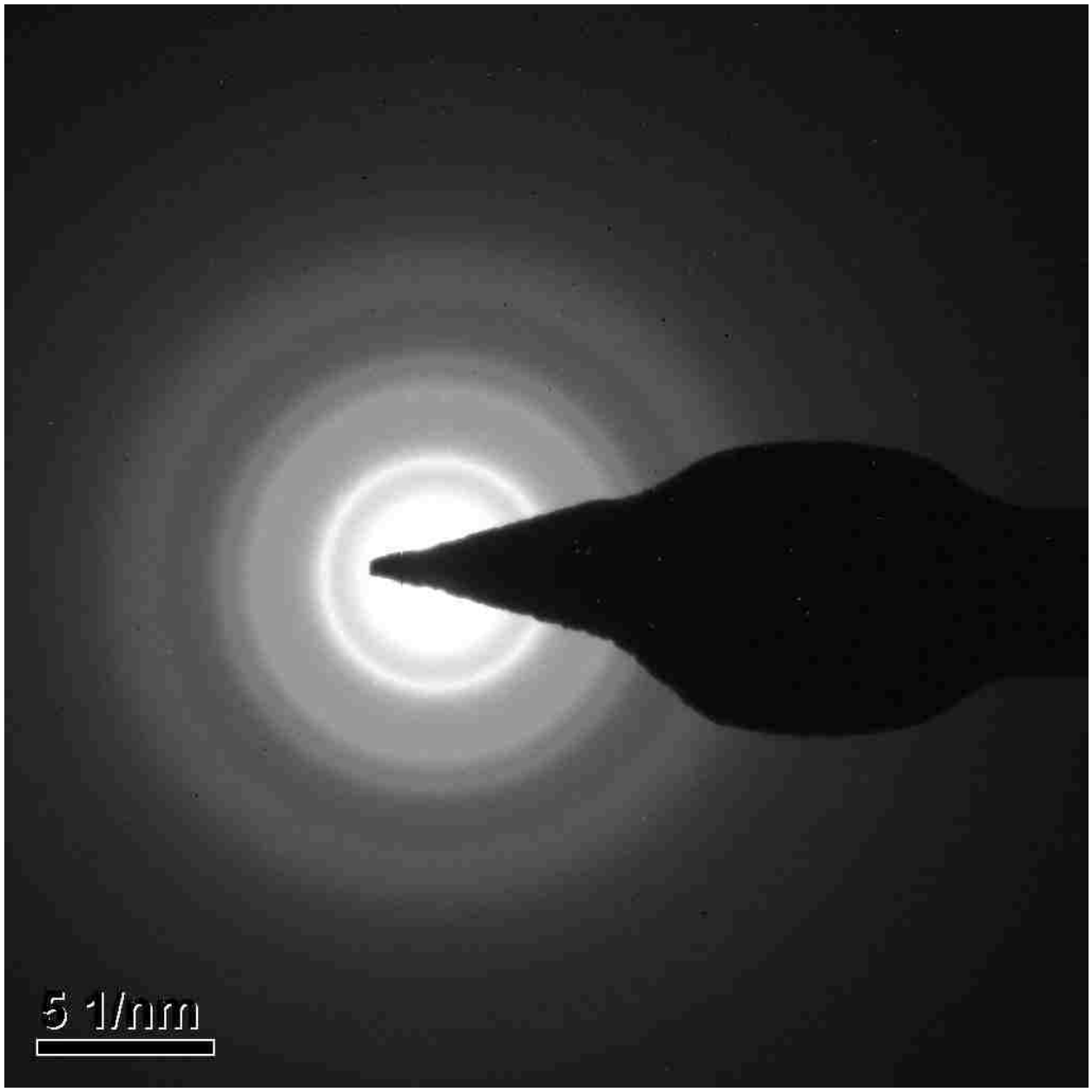

Figure 31- Selected area electron diffraction (SAED) image during HR-TEM of DHLA coated ZnS:Mn/ZnS Qdots showing the crystallinity

Lattice spacings ~3.09 Å, ~1.90 Å, and ~1.59 Å

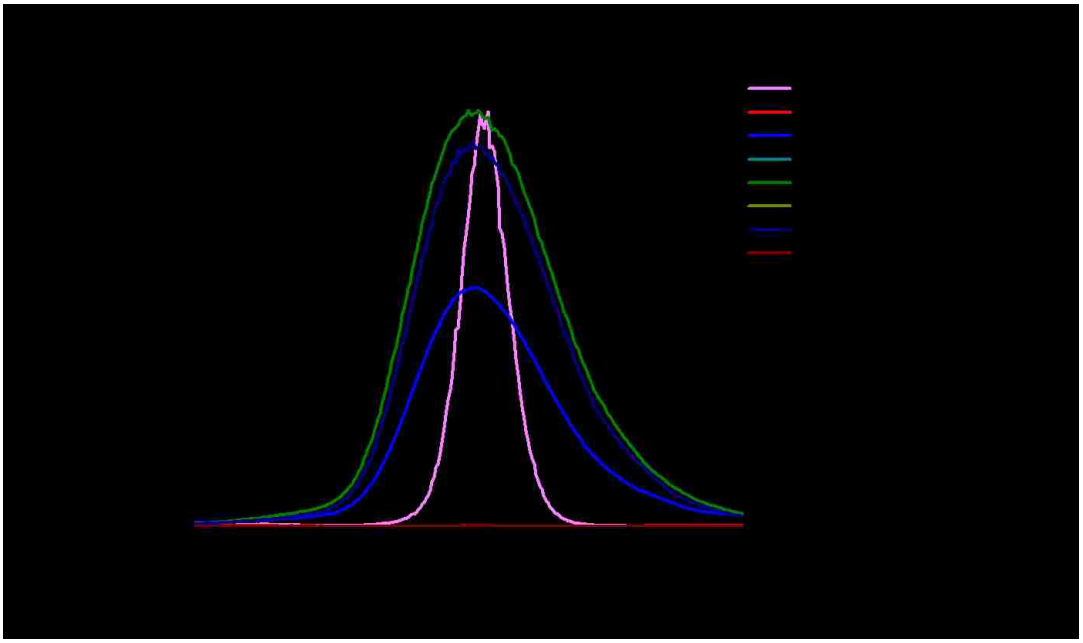

Figure 32- Fluorescence spectroscopy of normal and HCl treated (compromised) CdS:Mn/ZnS Qdots and commercial Qdot

Excitation λ: 375nm

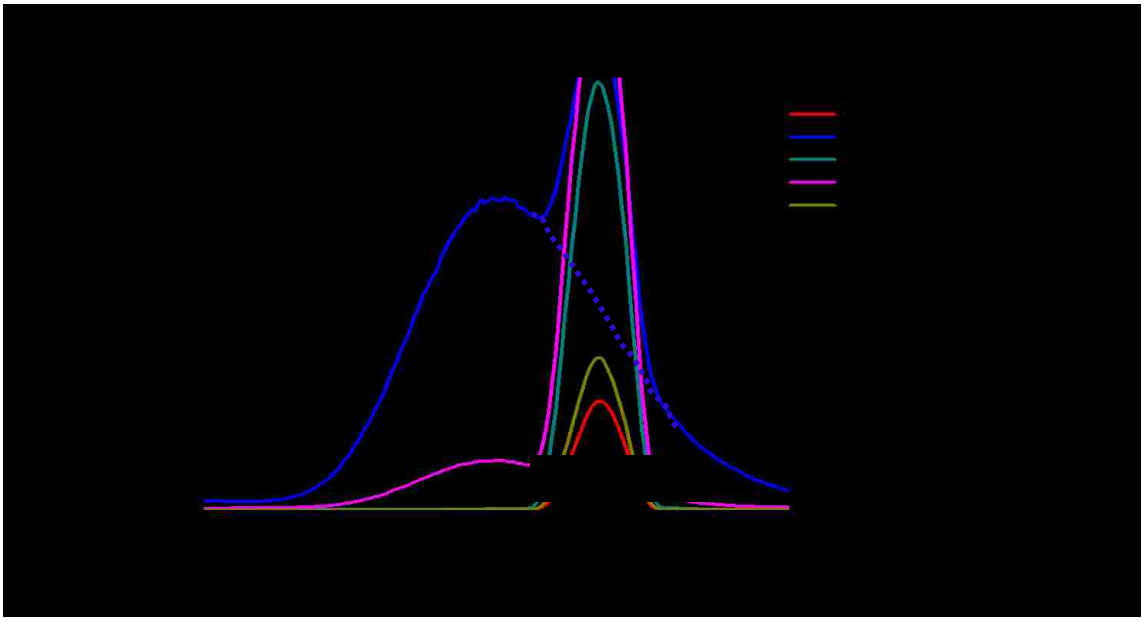

Figure 33- Fluorescence spectroscopy of normal and HCl treated (compromised) ZnS:Mn/ZnS Qdots

Excitation λ: 308nm

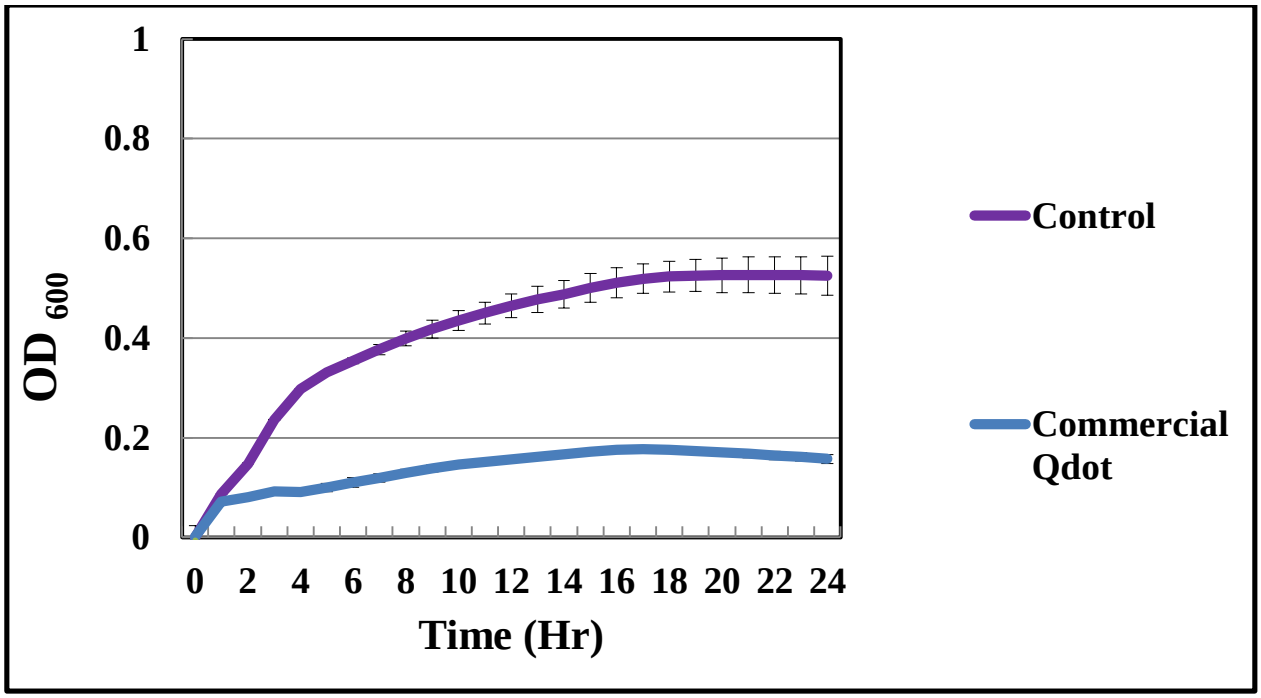

Figure 34- E. coli growth curve comparison between commercial Qdot (CdSe/ZnS) treated and non treated control.

Qdot metallic content 0.1 µg

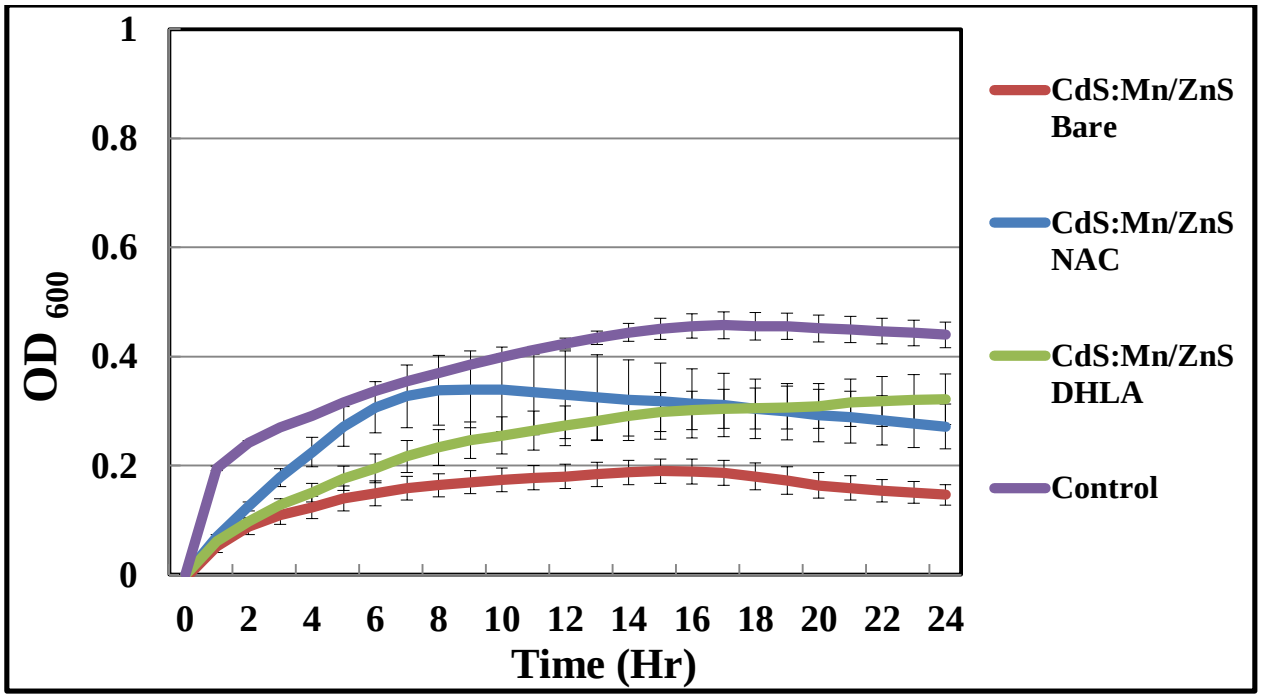

Figure 35- *E. coli g*rowth curve comparison with CdS:Mn/ZnS Qdots treated and untreated control.

Total metallic Cd 8.3µg

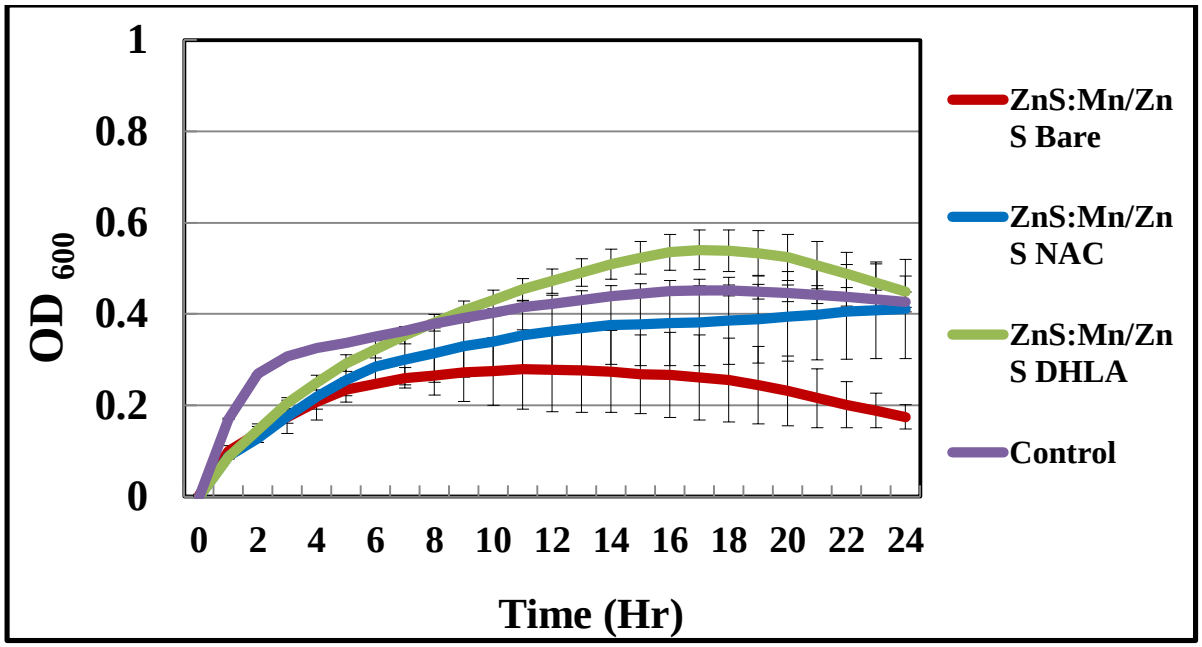

Figure 36- *E. coli* growth curve comparison with ZnS:Mn/ZnS Qdots treated and untreated control.

Total metallic Zn 38.9 µg

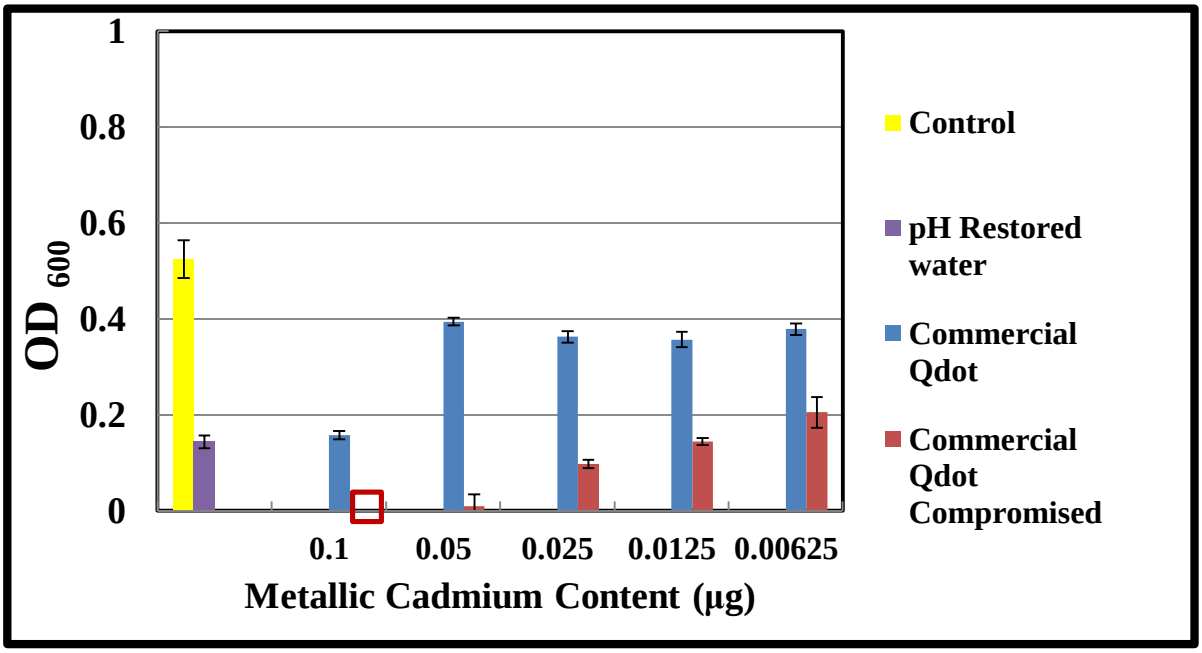

Figure 37- Endpoint turbidity comparison of normal and compromised commercial Qdots

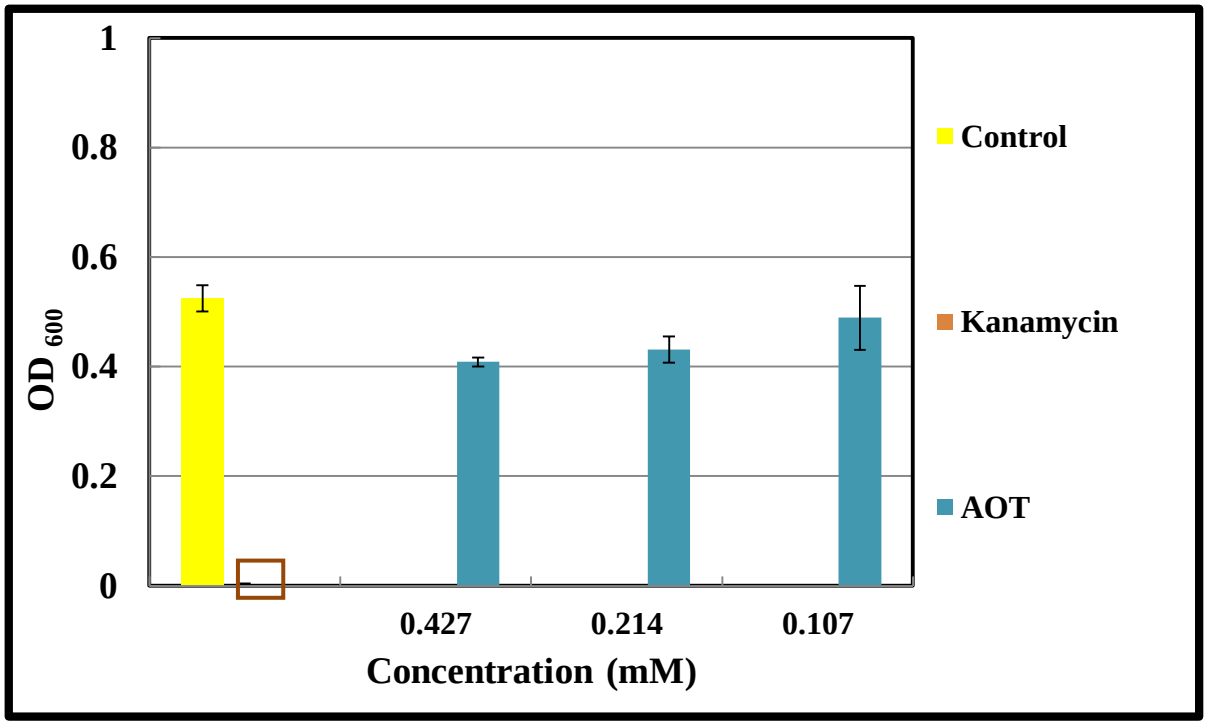

Figure 38- Endpoint turbidity comparison of AOT to untreated *E. coli*

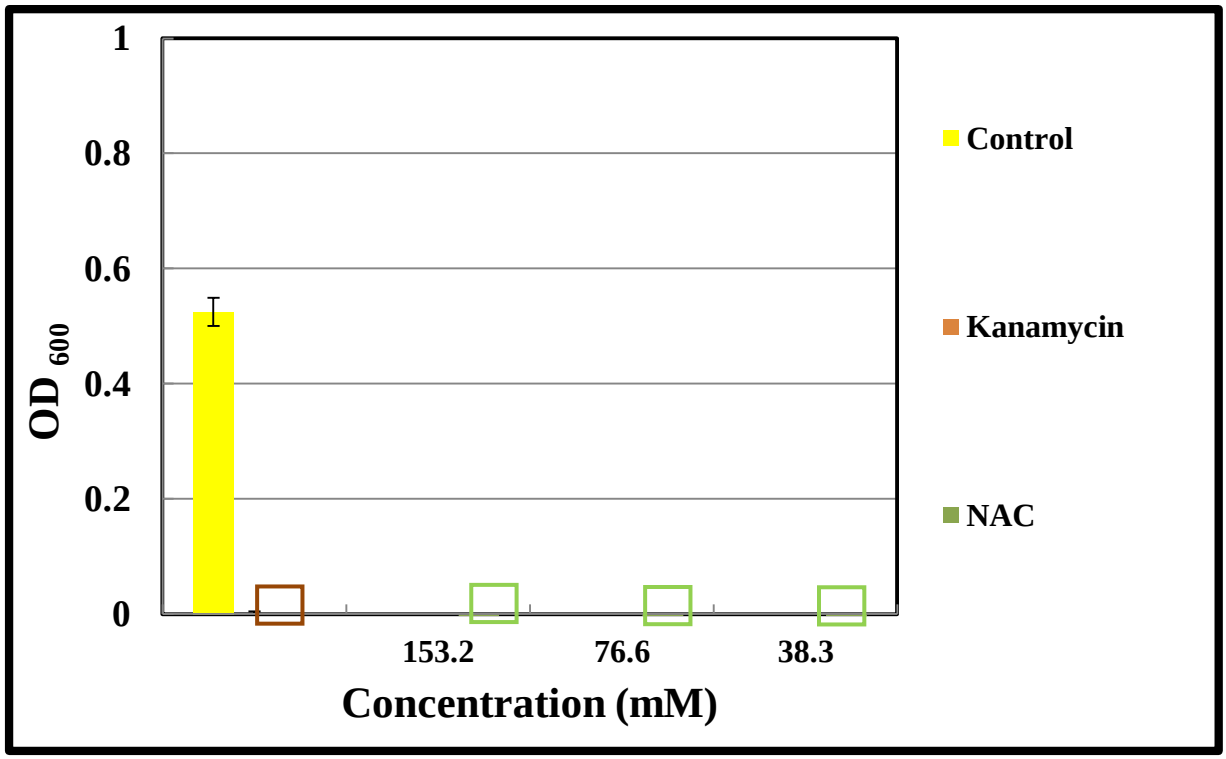

Figure 39- Endpoint turbidity comparison of NAC to untreated *E. coli*

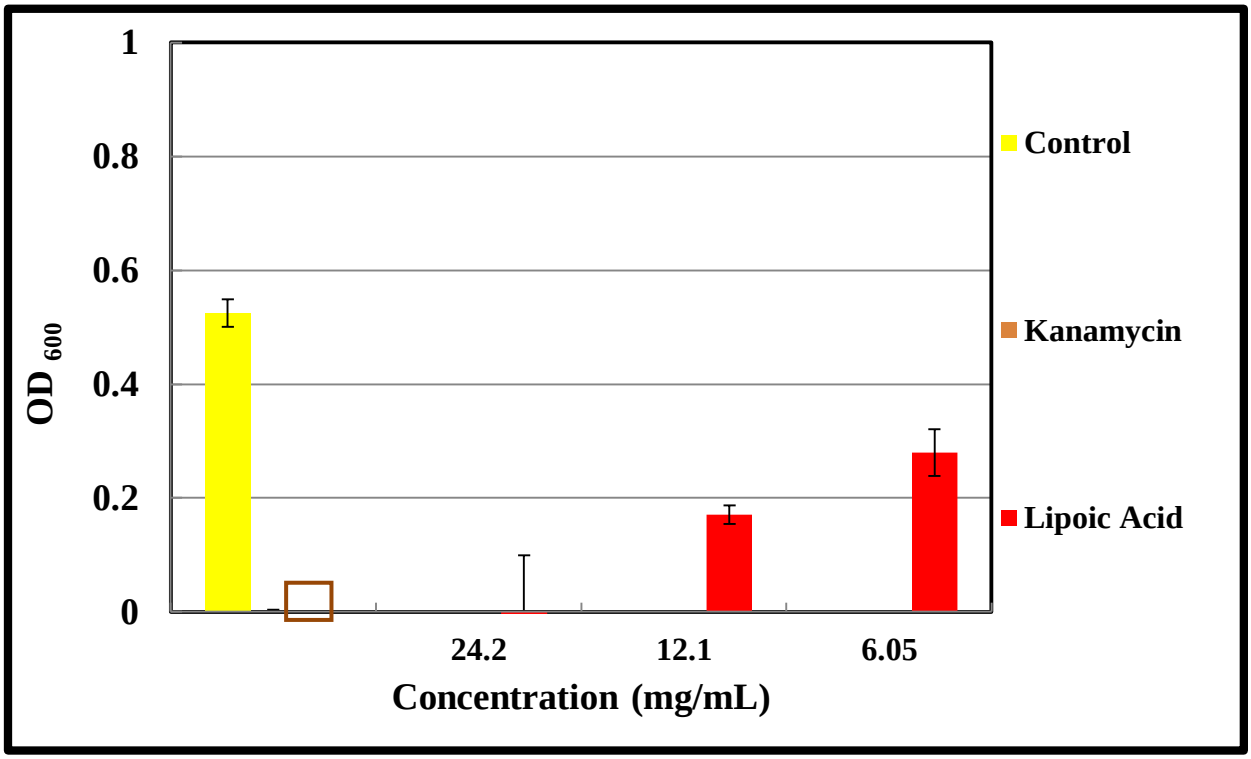

Figure 40- Endpoint turbidity comparison of AOT to untreated *E. coli*

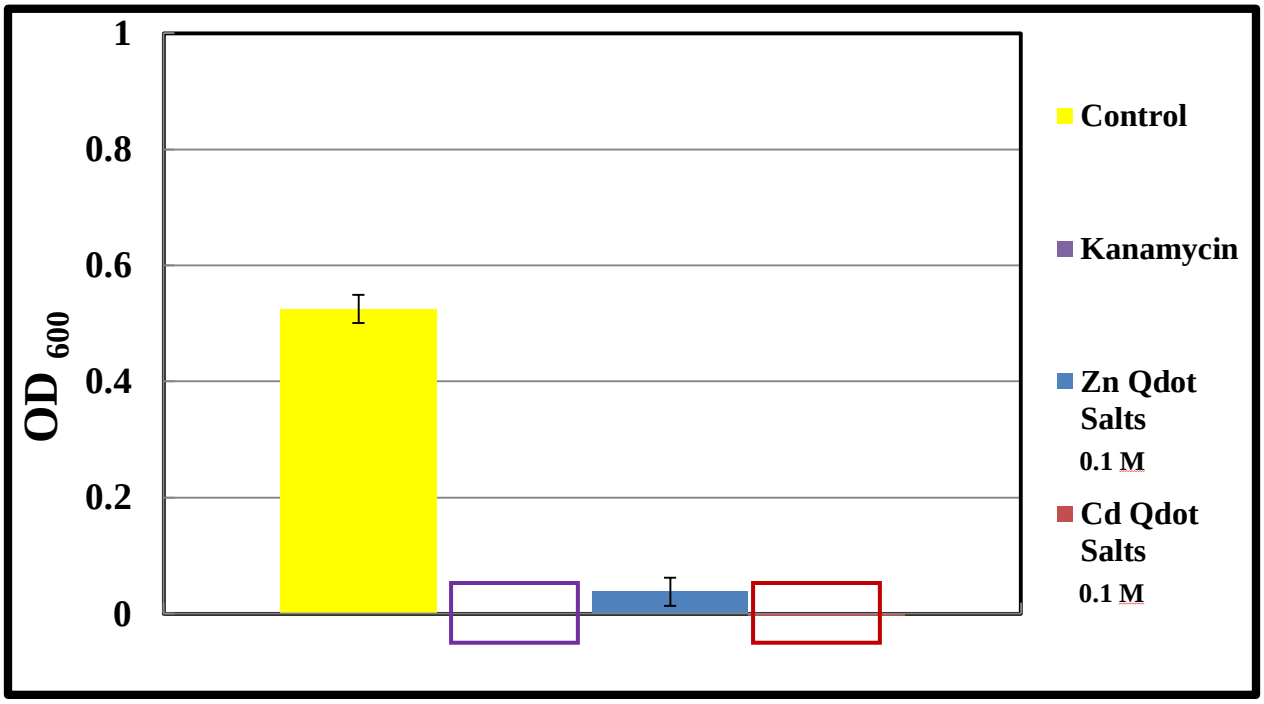

Figure 41- Endpoint turbidity comparison of Zinc acetate and Cadmium acetate salts to untreated E.coli

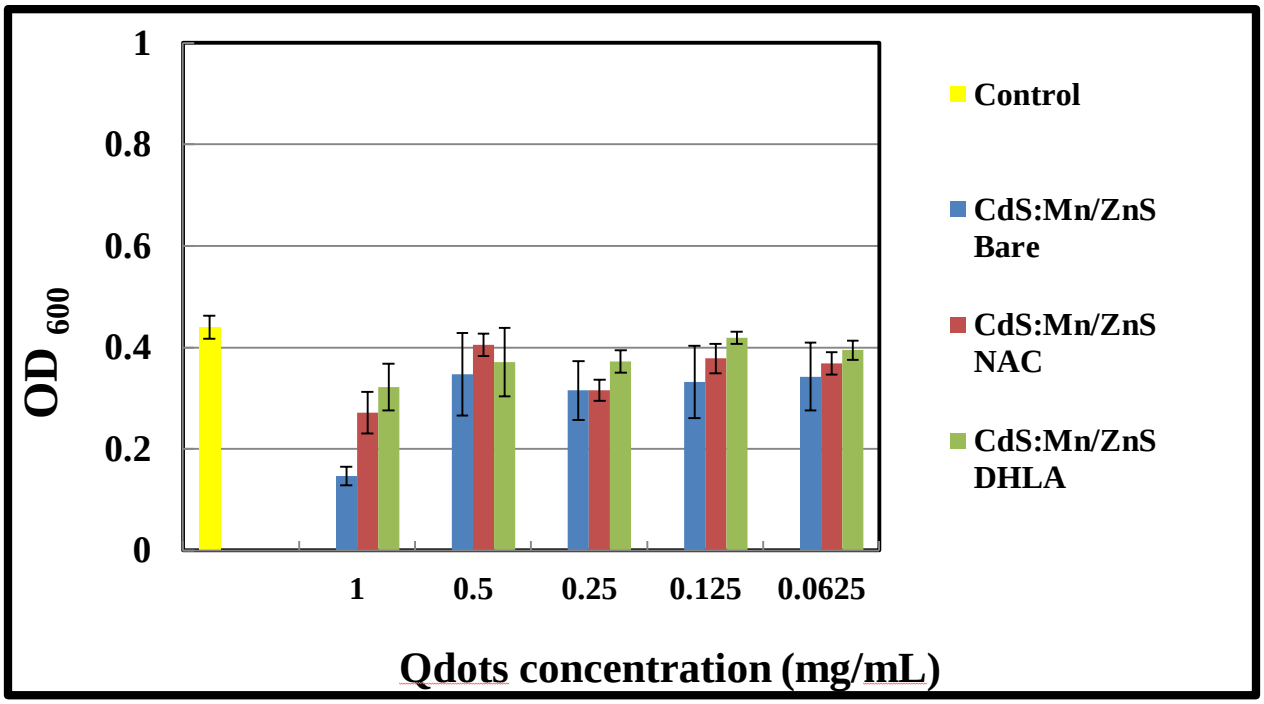

Figure 42- Endpoint turbidity comparison of CdS:Mn/ZnS Qdots

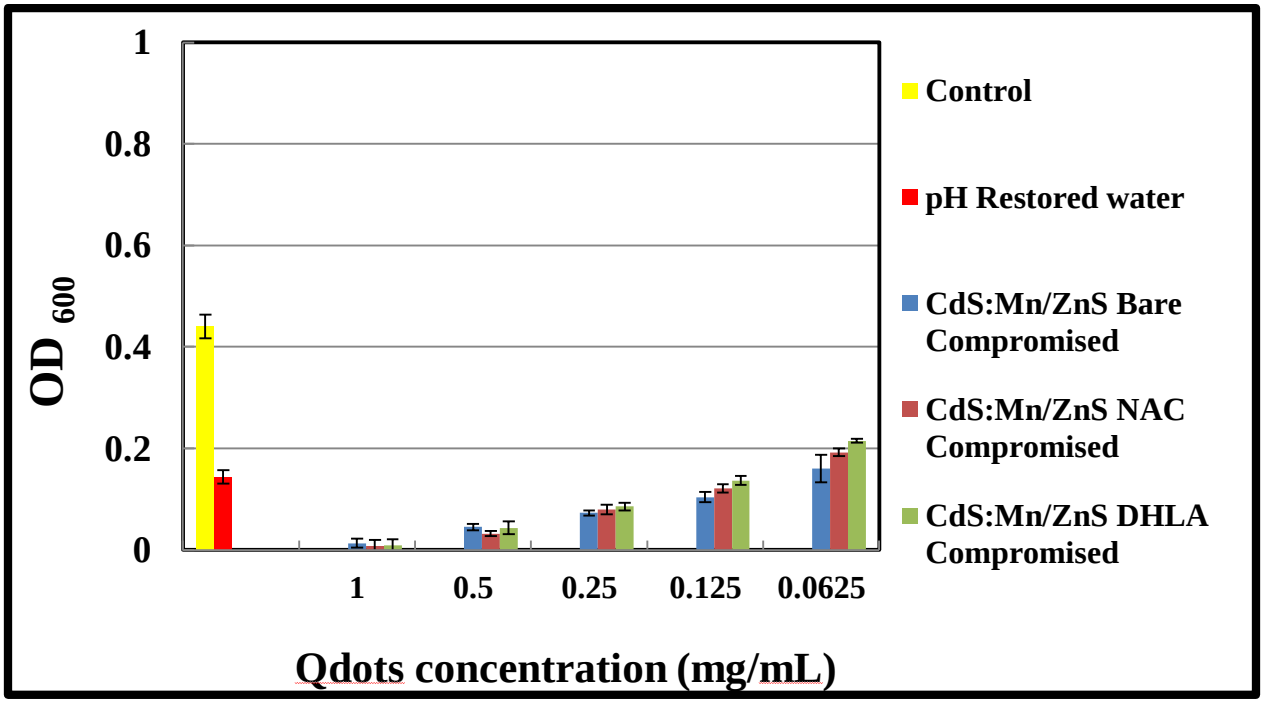

Figure 43- Endpoint turbidity comparison of compromised CdS:Mn/ZnS Qdots

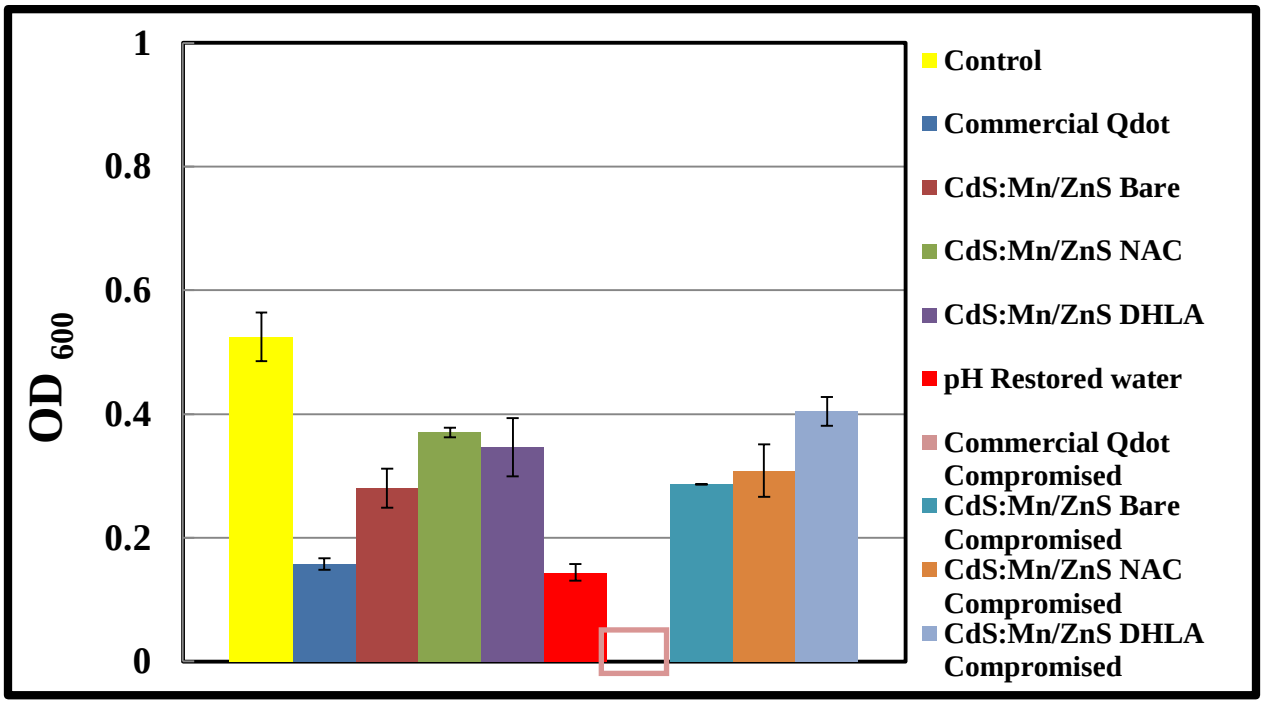

Figure 44- Endpoint turbidity of *E. coli* treated with commercial and synthesized Cadmium based Qdots, both normal and compromised.

Total metallic cadmium was normalized to 0.1µg for each Qdot sample

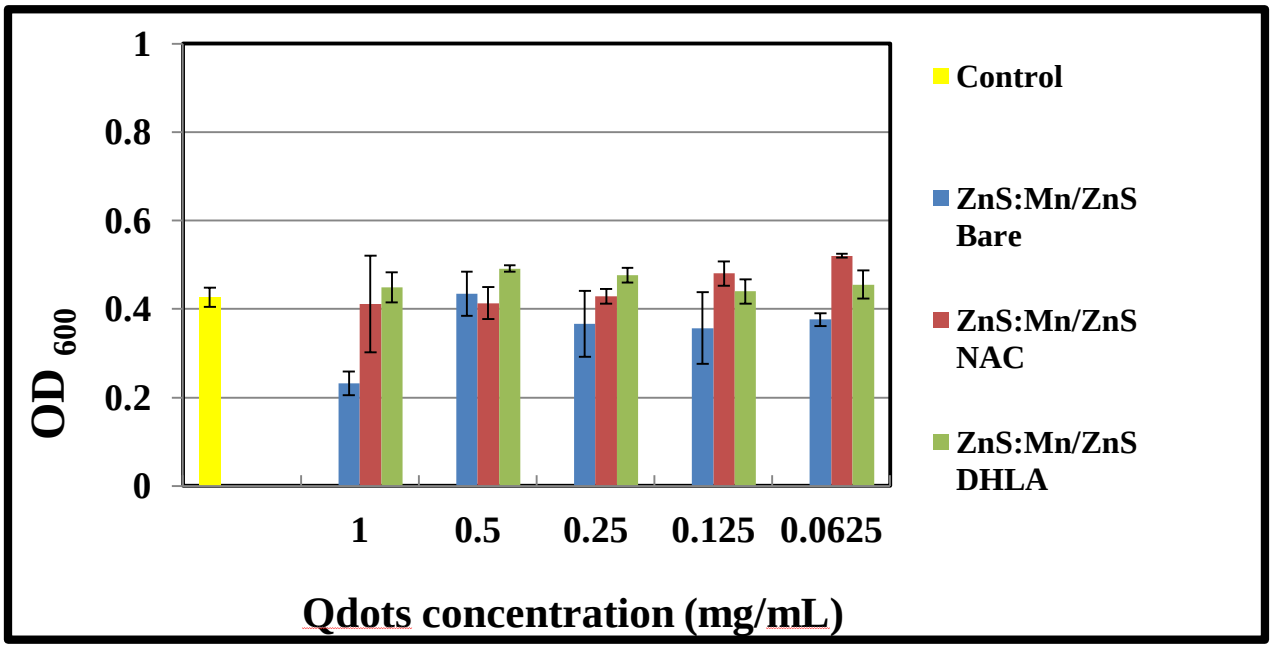

Figure 45- Endpoint turbidity comparison of ZnS:Mn/ZnS Qdots

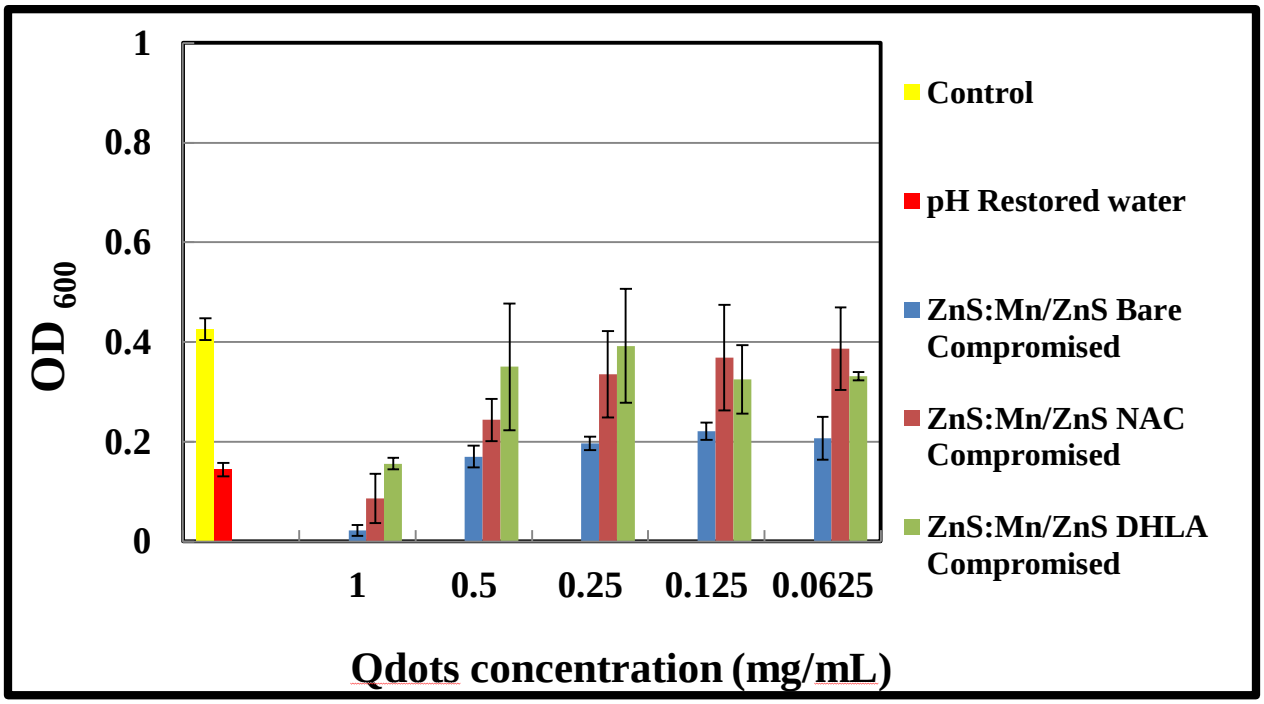

Figure 46- Endpoint turbidity comparison of compromised ZnS:Mn/ZnS Qdots

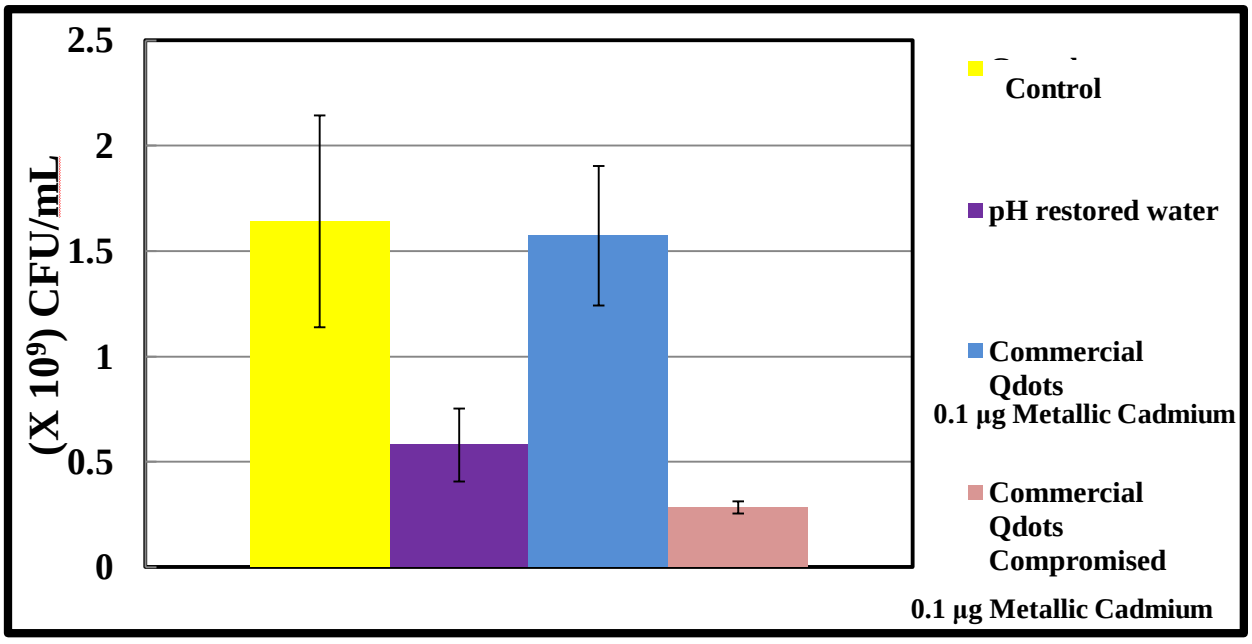

Figure 47- Colony counts of *E. coli* in the presence of normal and compromised commercial Qdots (0.1 µg of metallic cadmium)

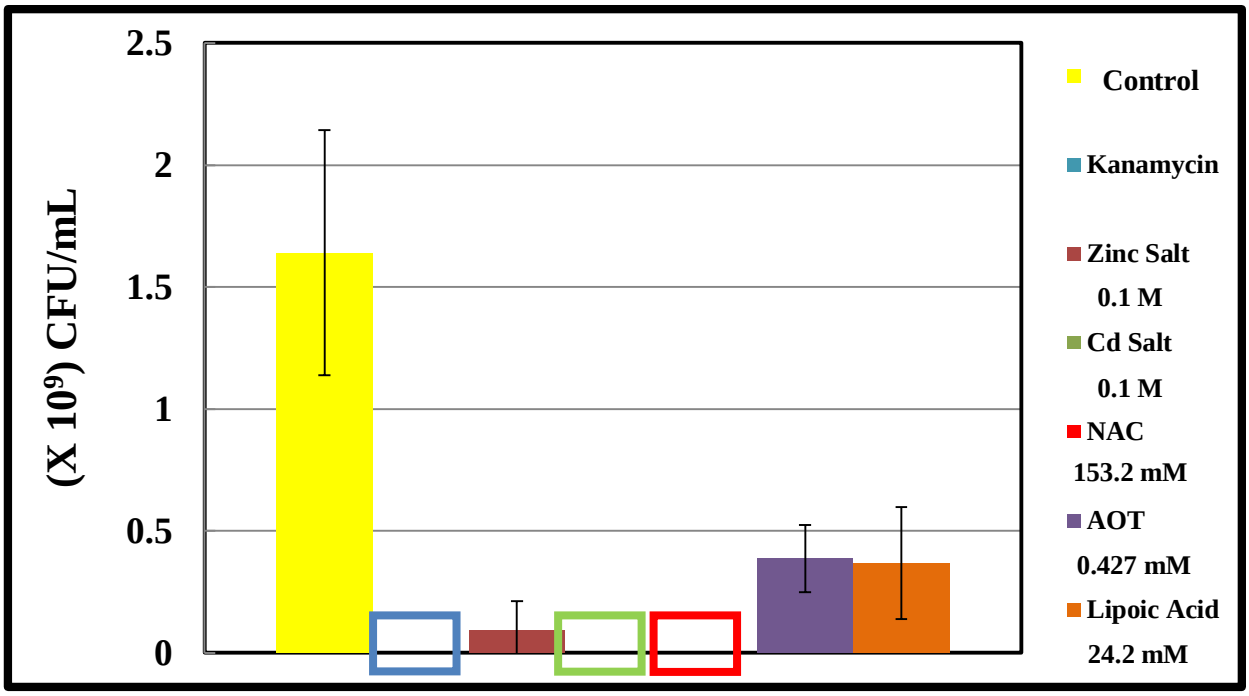

Figure 48- Colony count of *E. coli* untreated (control) compared to Qdot surface agents and core salts.

Kanamycin (30 µg/mL) control for bacterial killing

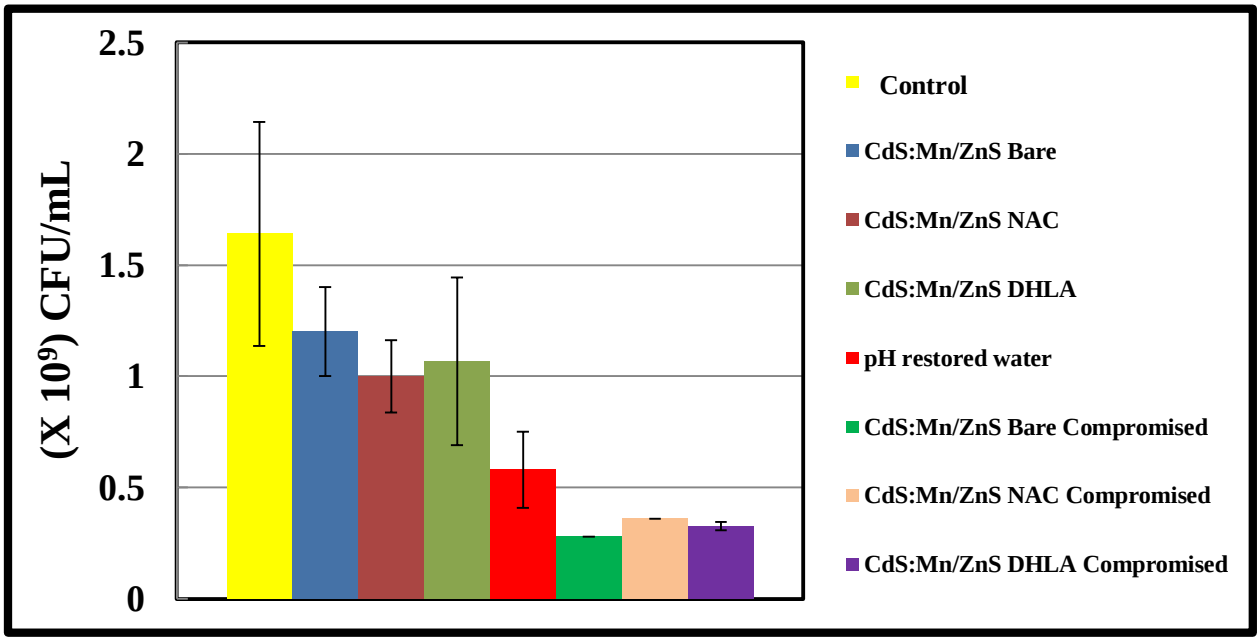

Figure 49- Colony counts of *E. coli* treated with normal and compromised CdS:Mn/ZnS Qdots

Total metallic Cd is 8.3 µg in each Qdot sample

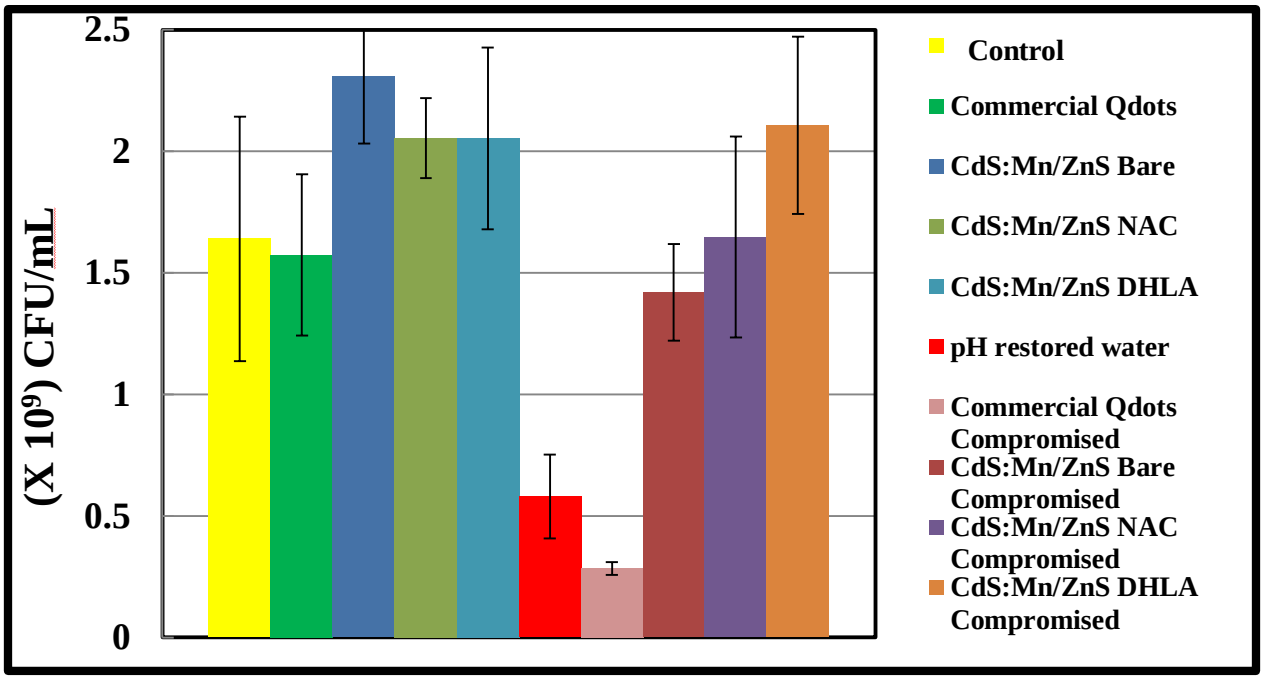

Figure 50- Colony counts of *E. coli* treated with commercial and synthesized Cadmium based Qdots, both normal and compromised.

Total metallic cadmium was normalized to 0.1µg for each Qdot sample

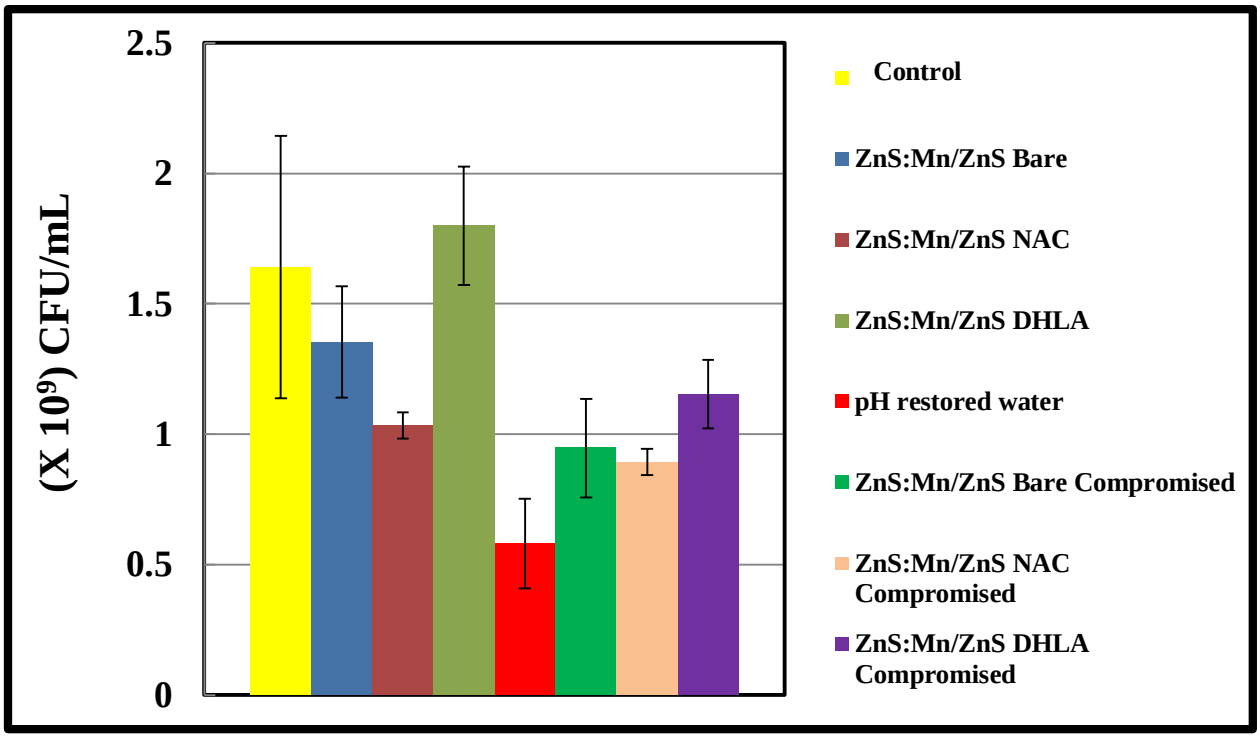

Figure 51- Colony forming units of *E. coli* treated with ZnS:Mn/ZnS Qdots and compromised ZnS:Mn/ZnS Qdots.

Total metallic zinc is 38.9 µg for each Qdot sample

CHAPTER 4- CONCLUSION

In the present work, HM free ZnS:Mn/ZnS and HM CdS:Mn/ZnS Qdots were successfully synthesized, modified and characterized. Quantum yield calculations were comparable to previously reported values. Surface modification improved Qdot absorption and fluorescence emission. Zeta potential measurements and NMR confirmed colloidal dispersion and surface functionality. HRTEM measured the crystal size to be between 3-5nm, and confirmed crystallinity of the nanoparticles. Qdot potential toxicity was evaluated using 6N HCl to simulate weathering, and *E. coli* was used as the model organism to assess toxicity. Growth inhibition and turbidity results indicated that Zn based Qdots exhibit a significantly less inhibitory effect on *E. coli* growth compared to Cd based Qdots. Synthesized surface modified Cd based Qdots are less toxic than commercial Qdots. Bactericidal assay results show that when the Qdots are compromised, Zn based Qdots and Qdots with antioxidant surface modifications will have less toxic effects than Cd based and unconjugated Cd based Qdots. Overall, Zn based Qdots, bare or surface modified, are less toxic to *E. coli* than Cd based Qdots. Since these results are only an indication of potential Qdot toxicity, further studies using other bacteria species are necessary to completely evaluate the negative environmental impact that compromised Qdots could have.

REFERENCES

1. Igor L. Medintz, H.T.U., Ellen R. Goldman, and Hedi Mattoussi, *Quantum Dot bioconjugates for imaging, labelling, and sensing.* Nature Materials, 2005. **4**.
2. Leevy, W.M., et al., *Quantum dot probes for bacteria distinguish Escherichia coli mutants and permit in vivo imaging.* Chemical Communications, 2008(20): p. 2331-2333.
3. Baruah, S., et al., *Manganese Doped Zinc Sulfide Quantum Dots for Detection of Escherichia coli.* Journal of Fluorescence. **22**(1): p. 403-408.
4. Rajendra N. Mitra, M.D., Xiaolei Zhang, Jessica C. Tyus, Niclas Bengtsson, Steven Fletcher, Brent D.G. Page, James Turkson, Andre J. Gesquiere, Patrick T. Gunning, Glenn A. Walter, Swadeshmukul Santra, *An activatable multimodal.multifunctional nanoprobe for direct imaging of intracellular drug delivery.* Biomaterials, 2011. **33**: p. 1500-1508.
5. Subhash Banerjee, S.K., J. Manuel Perez, and Swadeshmukul Santra, *Quantum Dot-based OFF/ON Probe for Detection of Glutathione.* Journal of Physical Chemistry, 2009. **113**: p. 9659-9663.

6. Liu, Y., et al., *Bacteria-mediated in vivo delivery of quantum dots into solid tumor.* Biochemical and Biophysical Research Communications. **425**(4): p. 769-774.

7. Santra, S., et al., *Synthesis of water-dispersible fluorescent, radio-opaque, and paramagnetic CdS : Mn/ZnS quantum dots: A multifunctional probe for bioimaging.* Journal of the American Chemical Society, 2005. **127**(6): p. 1656-1657.

8. Rurack, K. and M. Spieles, *Fluorescence Quantum Yields of a Series of Red and Near-Infrared Dyes Emitting at 600â^'1000 nm.* Analytical Chemistry. **83**(4): p. 1232-1242.

9. Abdelhay Aboulaich, M.G., Lavinia Balan, Jaafar Ghanbajar, Ghouti Medjahdi, and Raphael Schneider, *Water-Based Route to Colloidal Mn-Doped ZnSe and Core/Shell ZnSe/ZnS Quantum Dots.* Inorganic Chemistry, 2010. **49**: p. 10940-10948.

10. Parak, R.A.S.a.W.J., *Surface modification, funcitonalization and bioconjugation of colloidal inorganic nanoparticles.* Philosophical Transactions of the Royal Society A, 2010. **368**: p. 1333-1383.

11. Brouwer, A.M., *Standards for photoluminescence quantum yield measurements in solution.* Pure Appl. Chem, 2011. **83**(12): p. 2213-2228.

12. Zhang, Y., et al., *Photoluminescence Quenching of CdSe Core/Shell Quantum Dots by Hole Transporting Materials.* The Journal of Physical Chemistry C, 2009. **113**(5): p. 1886-1890.

13. Holloway, H.Y.a.P.H., *Enhanced photoluminescence from CdS:Mn/ZnS core/shell quantum dots.* Applied Physics Letters, 2003. **82**.

14. Hao-Ying Lu, S.-Y.C., and Soon-Seng Tan, *The Low-Temperature Synthesis and Optical Properties of Near-White Light Emission Nanophosphors Based on Manganese-Doped Zinc Sulfide.* The Japan Society of Applied Physics, 2005. **44**(7A): p. 5282-5288.

15. Rita John, S.S.F., *Optical, Structural and Morphological Studies of Bean-Like ZnS Nanostructures by Aqueous Chemical Method.* Chalcogenide Letters, 2010. **7**(4): p. 269-273.

16. Heesun Yang, S.S., and Paul H. Holloway, *Syntheses and Applications of Mn-Doped II-VI Semiconductor Nanocrystals.* Journal of Nanoscience and Nanotechnology, 2005. **5**: p. 1364-1375.

17. Holloway, H.Y.a.P., *Efficient and Photostable ZnS-Passivated CdS:Mn Luminescent Nanocrystals.* Advanced Functional Materials, 2004. **14**(2): p. 154-156.

18. Saydi, A.S.a.H., *A Theoretical Approach for Estimation of Ultimate Size of Bimetallic Nanocomposites Synthesized in Microemulsion Systems.* Russian Journal of Physical Chemistry A, 2012. **86**(13): p. 2014-2017.

19. S.K. Mehta, K.K., Shweta Sharma, K.K. Bhasin, *Behavior of acetyl modified amino acids in reverse micelles: A noninvasive and physiochemical approach.* Journal of Colloid and Interface Science, 2007(314): p. 689-698.

20. Xin Ai, Q.X., Marcus Jones, Qing Song, Shi-you Ding, Randy J Ellingson, Mike Himmel, Garry Rumbles, *Photophysics of (CdSe)ZnS colloidal quantum dots in an aqueous environment stabilized with amino acids and genetically-modified proteins.* Photochemical and Photobiological Sciences, 2007. **6**: p. 1027-1033.

21. Hedi Mattoussi, J.M.M., Ellen R. Goldman, George P. Anderson, Vikram C. Sundar, Frederic V. Mikulec, and Moungi G. Bawendi, *Self-Assembly of CdSe-ZnS Quantum Dot Bioconjugates Using an Engineered Recombinant Protein.* Journal of American Chemical Society, 2000(122): p. 12142-12150.

22. Anna M Sadowska, J.V., K Darquennes, WA De Backer, *Role of N-Acetylcysteine in the management of COPD.* Therapeutics and Clinical Risk Management, 2006. **2**(1): p. 3-18.

23. Moini, H., L. Packer, and N.-E.L. Saris, *Antioxidant and Prooxidant Activities of Î±-Lipoic Acid and Dihydrolipoic Acid.* Toxicology and Applied Pharmacology, 2002. **182**(1): p. 84-90.

24. Jawali, M.G.a.N., *N-Acetylcysteine-Mediated Modulation of Bacterial Antibiotic Susceptibility.* Antimicrobial Agents and Chemotherapy, 2010. **54**(8): p. 3529-3530.

25. Dan Zhao, Z.H., W.H. Chan, and Martin M. F. Choi, *Synthesis and Characterization of High-Quality Water-Soluble Near-Infrared-Emitting CdTe/CdS Quantum Dots capped by N-Acetyl -L-Cysteine Via Hydrothermal Method.* Journal of Physical Chemistry, 2009(113): p. 1293-1300.

26. Jie Cao, B.X., Hui Li, Dawei Deng, Yueqing Gu, *Facile Synthesis of high-quality water-soluble N-acetyl-L-cysteine-capped Zn1-xCdxSe/ZnS core/shell quantum dots emitting in the violet-green spectral range.* Journal of Colloid and Interface Science, 2010(348): p. 369-376.

27. Ann-Cathrin Olofsson, M.H., and Hans Elwing, *N-Acetyl-L-Cysteine Affects Growth, Extracellular Polusaccharide Production, and Bacterial Biofilm Formation on Solid Surfaces.* Applied and Environmental Microbiology, 2003. **69**(8): p. 4814-4822.

28. Liu, T.Z.a.Y., *N-acetylcysteine inhibit biofilms produced by Pseudomonas aeruginosa.* BMC Microbiology. 2010. **10**(140).

29. Lovell, M.A., et al., *Protection against amyloid beta peptide and iron/hydrogen peroxide toxicity by alpha lipoic acid.* Journal of Alzheimer's Disease, 2003. **5**(3): p. 229-239.

30. Rezk, B.M., et al., *Lipoic Acid Protects Efficiently Only against a Specific Form of Peroxynitrite-induced Damage.* Journal of Biological Chemistry, 2004. **279**(11): p. 9693-9697.

31. Coleman, M.D., C. Williams, and G.R.M.M. Haenen, *Effects of Lipoic Acid and Dihydrolipoic Acid on 4-Aminophenol-Mediated Erythrocytic Toxicity in vitro.* Basic & Clinical Pharmacology & Toxicology, 2006. **99**(3): p. 225-229.

32. Kang, H.-Y., *Review of Emerging Nanotechnology Industry: Materials, Fabrications, and Applications*. 2010, Department of Toxic Substances Control Pollution Prevention and Green Technology: CA.

33. *Municipal Solid Waste in the United States: 2011 Facts and Figures* 2011, US EPA. p. 67-72.

34. Hossain, Z. and F. Huq, *Studies on the interaction between Cd2+ ions and DNA.* Journal of Inorganic Biochemistry, 2002. **90**: p. 85-96.

35. Lee, J.M., Shaily; Alvarez, Pedro J.J, *Nanomaterials in the Constructions Industry: A review of their applications and environmental health and safety considerations.* ACS Nano, 2010. **4**(7): p. 3580-3591.

36. Wiecinski, P.N., et al., *Toxicity of Oxidatively Degraded Quantum Dots to Developing Zebrafish (Danio rerio).* Environmental Science & Technology. **47**(16): p. 9132-9139.

37. Lu Lai, C.L., Chang-qing Xiao, Zi-Qiang Xu, Xiao-Le Han, Li Fu, Dong-Wei Li, Ping Mei, Feng-Lei Jiang, Qing-Lian Guo, Yi Liu, *Adhesion of quantum dots-induced membrane damage of Escherichia coli.* Journal of Colloid and Interface Science, 2012(389): p. 61-70.

38. Shaily Mahendra, H.Z., Vicki L. Colvin, and Pedro J. Alvarez, *Quantum Dot Weathering Results in Microbial Toxicity.* Environmental Science and Technology, 2008. **42**: p. 9424-9430.

39. Yang, Y., et al., *Defense Mechanisms of Pseudomonas aeruginosa PAO1 against Quantum Dots and Their Released Heavy Metals.* ACS Nano. **6**(7): p. 6091-6098.

40. Yang, Y., et al., *Relative Susceptibility and Transcriptional Response of Nitrogen Cycling Bacteria to Quantum Dots.* Environmental Science & Technology. **46**(6): p. 3433-3441.

41. Sealy, C., *Weathering the risks of quantum dots.* Nano Today, 2009. **4**(2): p. 107-108.

42. McDevitt, C.A., et al., *A Molecular Mechanism for Bacterial Susceptibility to Zinc.* PLoS Pathogens, 2011. **7**(11): p. 1-9.

43. Allen, M.W., *Measurement of Fluorescence Quantum Yields*. 2010, Thermo Fisher Scientific. p. 4.

44. *Zeta Potential Theory*, in *Zetasizer Nano Series*.